

## Catalog of gamma-ray glows during four winter seasons in Japan

Y. Wada <sup>1,2,\*</sup>, T. Matsumoto,<sup>3</sup> T. Enoto <sup>2</sup>, K. Nakazawa,<sup>4</sup> T. Yuasa <sup>5</sup>, Y. Furuta,<sup>6</sup> D. Yonetoku,<sup>7</sup> T. Sawano,<sup>8</sup> G. Okada <sup>9</sup>,  
H. Nanto,<sup>9</sup> S. Hisadomi,<sup>10</sup> Y. Tsuji,<sup>10</sup> G. S. Diniz <sup>2</sup>, K. Makishima <sup>3,11,12</sup> and H. Tsuchiya <sup>13</sup>

<sup>1</sup>*Division of Electrical, Electronic and Infocommunications Engineering, Graduate School of Engineering, Osaka University, 2-1 Yamadaoka, Suita, Osaka 565-0871, Japan*

<sup>2</sup>*Extreme Natural Phenomena RIKEN Hakubi Research Team, Cluster for Pioneering Research, RIKEN, 2-1 Hirosawa, Wako, Saitama 351-0198, Japan*

<sup>3</sup>*Department of Physics, Graduate School of Science, The University of Tokyo, 7-3-1 Hongo, Bunkyo-ku, Tokyo 113-0033, Japan*

<sup>4</sup>*Kobayashi-Maskawa Institute for the Origin of Particles and the Universe, Nagoya University, Furo-cho, Chikusa-ku, Nagoya, Aichi 464-8601, Japan*

<sup>5</sup>*Block 4B, Boon Tiong Road, Singapore 165004, Singapore*

<sup>6</sup>*CLEAR-PULSE Co., Ltd., 6-25-27 Chuo, Ota-ku, Tokyo 143-0024, Japan*

<sup>7</sup>*School of Mathematics and Physics, College of Science and Engineering, Kanazawa University, Kakuma-cho, Kanazawa, Ishikawa 920-1192, Japan*

<sup>8</sup>*Advanced Research Center for Space Science and Technology, Institute of Science and Engineering, Kanazawa University, Kakuma-cho, Kanazawa, Ishikawa 920-1192, Japan*

<sup>9</sup>*Co-creative Research Center of Industrial Science and Technology (CIST),*

*Kanazawa Institute of Technology, 3-1 Yatsukaho, Hakusan, Ishikawa 924-0838, Japan*

<sup>10</sup>*Division of Particle and Astrophysical Science, Graduate School of Science, Nagoya University, Furo-cho, Chikusa-ku, Nagoya, Aichi 464-8601, Japan*

<sup>11</sup>*High Energy Astrophysics Laboratory, Nishina Center for Accelerator-Based Science, RIKEN, 2-1 Hirosawa, Wako, Saitama 351-0198, Japan*

<sup>12</sup>*Kavli Institute for the Physics and Mathematics of the Universe, The University of Tokyo, 5-1-5 Kashiwa-no-ha, Kashiwa, Chiba 277-8683, Japan*

<sup>13</sup>*Nuclear Science and Engineering Center, Japan Atomic Energy Agency, 2-4 Shirakata, Tokai-mura, Naka-gun, Ibaraki 319-1195, Japan*



(Received 4 August 2021; accepted 26 October 2021; published 15 November 2021)

In 2015, the Gamma-Ray Observation of Winter Thunderstorms (GROWTH) collaboration launched a mapping observation campaign for high-energy atmospheric phenomena related to thunderstorms and lightning discharges. This campaign has developed a detection network of gamma rays with up to 10 radiation monitors installed in the cities of Kanazawa and Komatsu, Ishikawa Prefecture, Japan, where low-charge-center winter thunderstorms frequently occur. During four winter seasons from October 2016 to April 2020, a total of 70 gamma-ray glows, i.e., minute-lasting bursts of gamma rays originating from thunderclouds, were detected. Their average duration is 58.9 s. Among the detected events, 77% were observed at night. The gamma-ray glows can be classified into temporally symmetric, temporally asymmetric, and lightning-terminated types based on their count-rate histories. An averaged energy spectrum of the gamma-ray glows is well fitted with a power-law function with an exponential cutoff, whose photon index, cutoff energy, and flux are  $0.613 \pm 0.009$  MeV,  $4.68 \pm 0.04$  MeV, and  $(1.013 \pm 0.003) \times 10^{-5}$  erg cm<sup>-2</sup> s<sup>-1</sup> (0.2–20.0 MeV), respectively. The present paper provides a catalog of gamma-ray glows and their statistical analysis detected during winter thunderstorms in the Kanazawa and Komatsu areas.

DOI: [10.1103/PhysRevResearch.3.043117](https://doi.org/10.1103/PhysRevResearch.3.043117)

### I. INTRODUCTION

Strong electric fields inside thunderclouds have recently been recognized as a particle accelerator in nature. Gamma-

ray glows, also called thunderstorm ground enhancements (TGEs) when detected at the ground, are minute-lasting high-energy phenomena in the atmosphere caused by strong electric fields [1–4]. Electrons accelerated to a relativistic energy in an electric field emit bremsstrahlung photons by colliding with atmospheric atoms. The energy spectrum of gamma-ray glows typically extends up to tens of MeV [5,6], and their observed duration ranges from seconds to tens of minutes [5,7–9].

Since the first detection by an F-106 aircraft [1,10], gamma-ray glows have been detected via experiments

\*Corresponding author: [wada@yuuki-wd.space](mailto:wada@yuuki-wd.space)

Published by the American Physical Society under the terms of the [Creative Commons Attribution 4.0 International](https://creativecommons.org/licenses/by/4.0/) license. Further distribution of this work must maintain attribution to the author(s) and the published article's title, journal citation, and DOI.

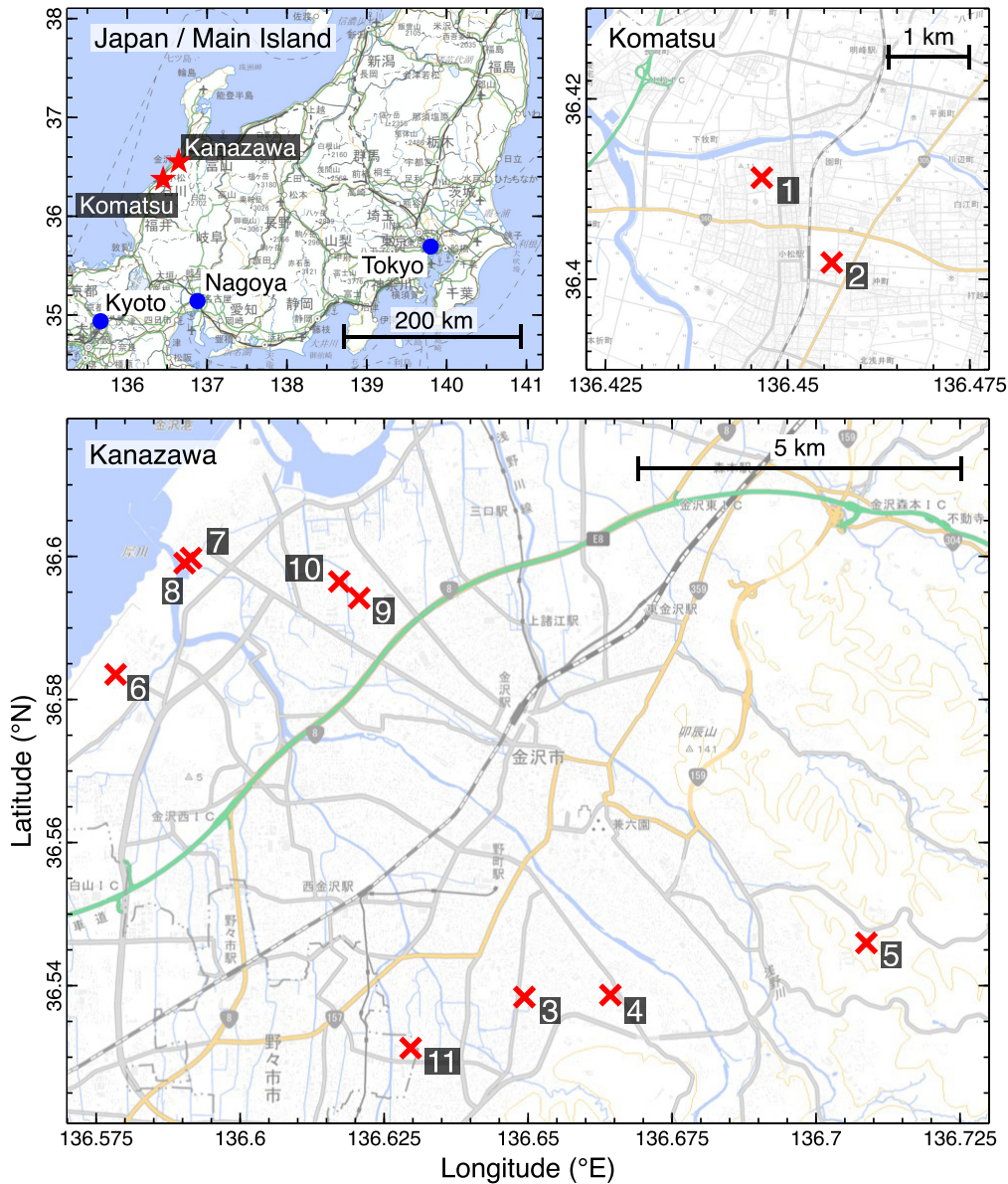


FIG. 1. Maps of observation sites. The red cross markers indicate the position of radiation monitors with their ID numbers. The background maps are provided by Geospatial Information Authority of Japan.

onboard balloons [11] and aircraft [7,12], and those located on a mountain [4,13] and at sea level [2,3,14]. Thanks to the recent advances in detectors, aircraft experiments have achieved precise measurements of gamma-ray glows inside or in the vicinity of thunderclouds [7,12,15,16]. At the same time, ground-based experiments have also contributed greatly to gamma-ray glow studies.

Mountain experiments are one of the important ways to study gamma-ray glows/TGEs at the ground. Electric fields of thunderclouds are usually formed at an altitude of 3 km or higher in summer. Gamma rays coming out from electric-field regions cannot reach sea level as they are absorbed by the atmosphere. Therefore, mountain experiments at an altitude of 2–3 km or higher are necessary for glow studies during summertime thunderstorms. So far, the following cosmic-ray observatories have observed gamma-ray glows: the Aragats Space Environmental Center

in Armenia [4,17,18]; Yangbajing in Tibet, China [8]; Mt. Norikura in Japan [19]; Tien Shan in Kazakhstan [20]; as well as the weather station at Mt. Fuji in Japan [13]. In particular, the Aragats Space Environmental Center has observed the largest number of TGEs in the world [9].

The other opportunities to detect gamma-ray glows at ground level are winter thunderstorms in Japan. When dry and cold seasonal winds come from a Siberian cold air mass over the Tsushima warm current, which is an active ascending air current, a thunderstorm can form in the northwest coast of Japan’s main island, called the “Hokuriku” region [26,27]. One of the important characteristics of these winter thunderstorms (distinguished from summer ones) is a low charge center. Precipitation particles that contribute to charging (i.e., ice crystals, graupels) are produced at an altitude whose temperature ranges from  $-10$  to  $0^\circ\text{C}$  or higher [28,29]. It typically corresponds to  $\sim 3$  km for summer

TABLE I. Specifications and observation periods of radiation monitors.

ID	Site	Crystal	Operation period			
			FY2016	FY2017	FY2018	FY2019
1	Komatsu High School (36.411°N, 136.446°E)	BGO	2016.10.13– 2017.04.03	2017.11.28– 2018.03.15	2018.11.08– 2019.03.27	2019.11.19– 2020.04.12
2	Science Hills Komatsu (36.402°N, 136.456°E)	BGO	2016.10.14– 2017.04.05	2017.11.30– 2018.03.15	2018.11.08– 2019.03.27	2019.11.19– 2020.04.12
3	Kanazawa Izumigaoka High School (36.538°N, 136.649°E)	BGO	2016.10.13– 2017.04.08	2017.11.27– 2018.03.04	2018.11.07– 2019.03.20	2019.11.18– 2020.04.12
4	Kanazawa University High School (36.539°N, 136.664°E)	BGO	2016.10.12– 2017.04.11	2017.11.30– 2018.03.12	2018.11.16– 2019.03.25	2019.11.18– 2020.04.12
5	Kanazawa University (36.546°N, 136.709°E)	BGO	2016.10.10– 2017.04.15	2017.12.01– 2018.03.12	2018.11.08– 2019.03.26	2019.11.20– 2020.04.12
6	Ishikawa Plating Industry Senkoji Plant (36.583°N, 136.578°E)	CsI		2017.11.29– 2018.03.09	2018.11.06– 2019.03.27	2019.11.20– 2020.04.12
7	Ishikawa Plating Industry Head Quarter (36.6°N, 136.591°E)	CsI		2017.11.29– 2018.03.09		2019.11.20– 2020.04.12
8	Ishikawa Plating Industry Second Plant (36.599°N, 136.59°E)	CsI		2017.11.29– 2018.03.09	2018.11.06– 2019.03.27	
9	Industrial Research Institute of Ishikawa (36.594°N, 136.621°E)	CsI			2018.12.05– 2019.03.06	2019.11.19– 2020.04.15
10	Kanazawa Nishi High School (36.596°N, 136.617°E)	CsI			2018.11.07– 2019.01.01	2019.11.20– 2020.03.07
11	Kanazawa Institute of Technology (36.531°N, 136.63°E)	CsI			2018.12.21– 2019.03.27	2019.11.27– 2020.04.14

thunderstorms, but less than 1 km for winter ones [30]. Therefore, gamma rays emitted from winter thunderclouds can be detected even at sea level. High-energy emission from winter thunderstorms in Japan was discovered unexpectedly and has been investigated by radiation monitors in nuclear power stations [2,31]. Following these findings, we have performed a ground-based radiation measurement called the Gamma-Ray Observation of Winter Thunderclouds (GROWTH) experiment in the Hokuriku region beginning in 2006 [3,6,22,32–34].

Gamma-ray glows are thought to originate from strong electric fields formed within thunderclouds, not directly from lightning discharges. On the other hand, they are often quenched by nearby discharges since lightning currents could discharge the corresponding electric fields [1,6,7,18,32]. More rare cases of the association between gamma-ray glows and lightning discharges are terrestrial gamma-ray flashes (TGFs). TGFs are instantaneous gamma-ray emission coincident with lightning discharges [35–38]. Their duration is typically a few hundred microseconds [38,39], and their energy spectrum also extends up to  $>20$  MeV [36,40,41]. TGFs have been detected mainly by space-borne detectors such as CGRO [35], RHESSI [36], AGILE [37], Fermi [42], and ASIM [43]. While the TGFs observed from space are upward-going, downward TGFs have been recently detected by ground-based experiments [44–47]. In addition, a few cases of glow terminations coincided with downward TGFs [24,48]. The connection between gamma-ray glows and downward TGFs is one of the intriguing questions in this field.

One of the widely known theories of electron acceleration in the atmosphere is the theory of relativistic runaway electron avalanches (RREAs) [49]. When the strength of electric fields exceeds the RREA threshold ( $0.284 \text{ MV m}^{-1}$  at 1 atm [50,51]), seed electrons of hundreds of keV or several MeV can be accelerated up to tens of MeV, and they produce secondary electrons that are also accelerated. Therefore, the number of electrons can be multiplied exponentially in such a high electric field. The accelerated electrons can emit bremsstrahlung photons as they interact with ambient atmospheric atoms. The energetic seed electrons are thought to be provided by cosmic rays, for example. The multiplication processes can be further boosted by relativistic feedback processes [51,52], and in fact some bright glows are thought to require the feedback mechanism [7,24].

Even when the electric fields are less than the RREA threshold, electrons of a cosmic-ray origin can gain energies from the field while electron multiplication hardly takes place. The excess in energies from the normal cosmic-ray spectra can also be detected as fainter gamma-ray glows than those produced by RREAs. This mechanism is called modification of the energy spectrum (MOS) [17,53,54], and it is the other important process that explains gamma-ray glows [12,55].

In 2015, we launched a mapping observation campaign with multiple radiation monitors in the Hokuriku region [22]. Since the launch of that campaign, we have reported the discovery of photonuclear reactions triggered by a downward TGF [34], an observation of a glow termination

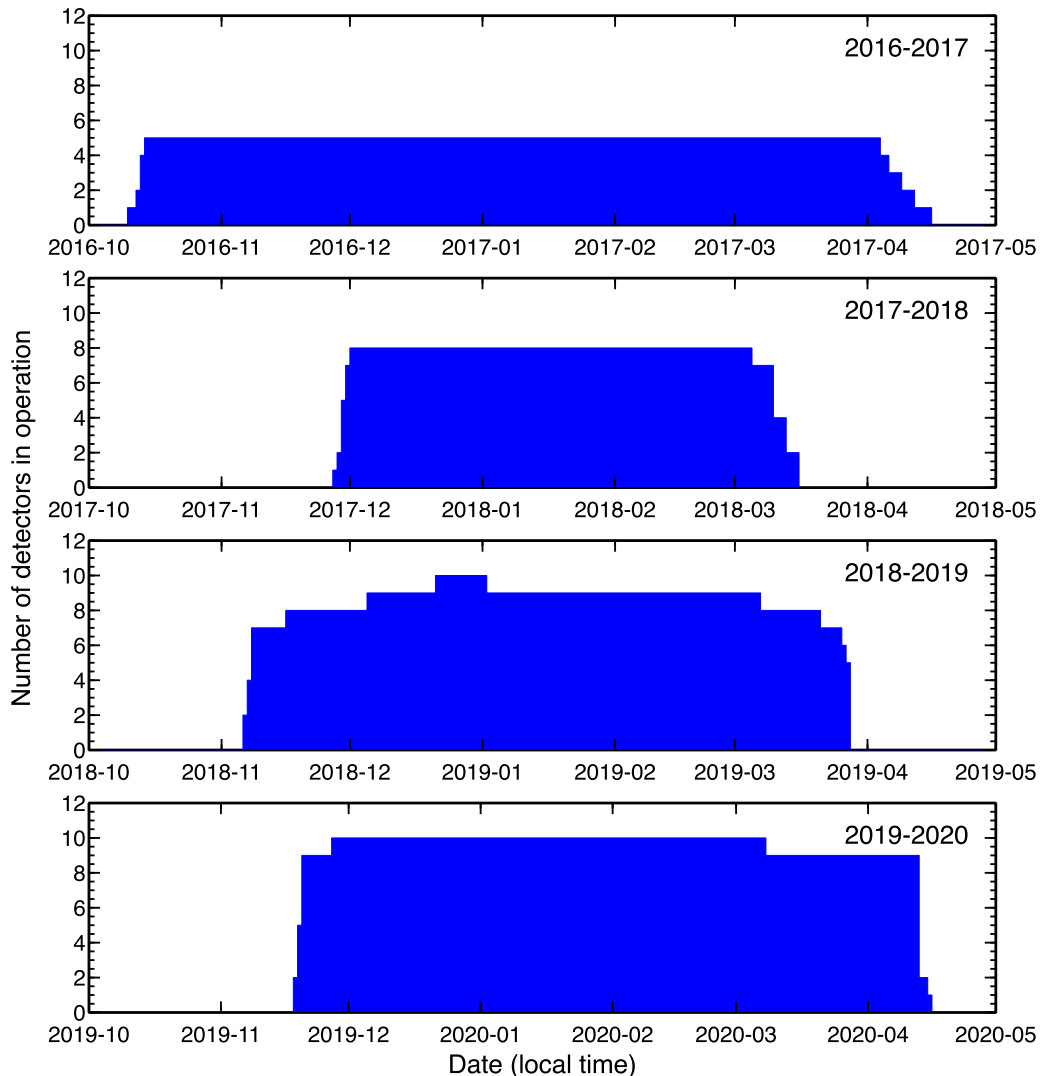


FIG. 2. Operation histories of the number of radiation detectors during the four winter seasons.

with radiofrequency lightning mapping and electric field measurements [6], the simultaneous detection of a glow termination and a downward TGF [24], and so on. In addition, more and more gamma-ray glows have been detected as the number of detectors increases. The present paper provides the first catalog of gamma-ray glows observed by the GROWTH collaboration during four winter seasons in Japan. Statistical investigations of occurrence rates and temporary and spectral features of gamma rays are presented. Throughout this paper, errors are at a confidence level of 1 standard deviation unless otherwise noted.

## II. OBSERVATION

Since 2006, we have operated an observation site at the Kashiwazaki-Kariwa nuclear power station of Tokyo Electric Power Company Holdings in Niigata Prefecture. In addition to the Kashiwazaki site, we established Kanazawa and Komatsu observation areas in Ishikawa Prefecture for the mapping observation campaign after 2015. Their locations are presented in Fig. 1. In the present paper, we focus on the results obtained at the Kanazawa and Komatsu areas because very few

gamma-ray glows have been detected at the Kashiwazaki site since 2015 despite several detections of downward TGFs and subsequent photonuclear reactions [34,47].

The Kanazawa and Komatsu sites have been developed since 2016, after a preliminary observation campaign in the 2015–2016 winter season. In the four winter seasons from 2016–2017 (FY2016; FY stands for Japanese fiscal year, from April to next March) to 2019–2020 (FY2019), two observation sites in Komatsu and nine sites in Kanazawa were in operation. The location and operation period of the observation sites are summarized in Table I. Four sites are located at high schools, two at universities, two at public facilities, and the rest at a private company. Limited by the number of radiation detectors, up to 10 observation sites were simultaneously in operation (in FY2018 and FY2019). Figure 2 shows the time histories of the number of detectors in operation during four winter seasons. In each winter season, observations typically start in October or November, then end in March or April. Therefore, the average operation duration is 4–5 months in each year.

Our radiation monitors consist of two types of scintillation crystals: a  $25.0 \times 8.0 \times 2.5$  cm<sup>3</sup> bismuth germanate

TABLE II. Event list of gamma-ray glows.

No.	Detection time (JST)	Site	Type <sup>a</sup>	Signif. <sup>b</sup>	Num. of photons	Duration (s)	Energy range (MeV)	Timing accuracy	Wind <sup>c</sup>		Temp. (°C)	Pub. <sup>d</sup>
									speed (m s <sup>-1</sup> )	direction (degree)		
1	2016/12/08 00:13:39	5	S	10.6	491±28	61	0.3–15	±0.5 s	9.5±1.2	260	7.2	[21]
2	2016/12/08 02:56:24	1	S	11.5	807±38	118	0.7–16	±0.5 s	10.9±1.2	300	5.9	[22]
3	2016/12/08 02:58:21	2	S	43.8	3421±38	98	0.4–14	±0.5 s	10.9±1.2	300	5.9	[22]
4	2016/12/09 16:29:03	3	T	9.2	326±24	43.5	0.7–14	±0.5 s	18.1±1.4	260	9.7	
5	2017/01/13 01:43:38	5	S	10.0	335±28	46	0.3–15	±0.5 s	20.1±2.2	260	5.7	[21]
6	2017/01/13 05:05:22	5	A	184.2	5236±28	42	0.3–14	±0.5 s	16.1±1.5	270	6.1	[21]
7	2017/01/15 05:30:47	5	S	12.0	522±28	56	0.3–14	±0.5 s	16.7±1	310	-0.4	[21]
8	2017/02/06 05:06:46	5	S	5.4	228±33	86	0.3–15	±0.5 s	16.5±1.1	260	6.8	[21]
9	2017/02/06 05:10:33	5	S	5.3	67±38	101	0.3–15	±0.5 s	16.5±1.1	260	6.8	[21]
10	2017/12/05 03:27:07	1	S	9.7	295±25	45	0.4–25	±1 s	13.2±1.3	250	6.8	
11	2017/12/05 03:27:39	2	S	8.9	168±26	35	0.4–23	±1 μs	13.2±1.3	250	6.8	
12	2017/12/05 11:51:43	6	S	15.5	454±24	38	0.4–24	±1 μs	20.2±1.4	240	5	
13	2017/12/05 12:07:13	1	S	74.1	2327±28	44	0.4–24	±1 s	21.6±1.2	240	4	
14	2017/12/05 18:33:38	5	A	14.0	1030±37	108	0.4–23	±1 μs	14.8±1	260	6.6	[21,23]
15	2017/12/11 17:49:01	3	T	24.4	936±23	45	0.4–20	unknown	21.6±1.1	250	4.9	
16	2017/12/11 17:49:01	4	T	98.9	1388±19	25.5	0.4–21	±1 μs	21.6±1.1	250	4.9	
17	2017/12/11 17:52:05	5	A	16.0	632±38	121	0.4–23	±1 μs	21.6±1.1	250	4.9	[21]
18	2017/12/11 18:17:39	5	S	4.7	N/A	N/A	0.4–23	±1 μs	21±1.2	250	4	
19	2017/12/26 08:10:12	3	S	124.3	3305±28	34.5	0.4–20	unknown	20.6±1.4	260	5.8	
20	2017/12/26 08:11:10	4	S	91.8	3239±27	39	0.4–21	±1 μs	20.6±1.4	260	5.8	
21	2018/01/03 03:19:36	3	S	11.8	251±21	24.5	0.4–20	unknown	11.8±1.2	290	2.7	
22	2018/01/09 23:41:36	2	A	112.7	6496±37	92	0.4–22	±1 μs	15.9±1.4	250	1.8	
23	2018/01/10 02:36:55	1	S	19.5	468±23	33	0.4–24	±1 s	20.4±1.3	250	1.6	
24	2018/01/10 02:53:54	3	S	123.7	3458±25	35.5	0.4–20	<1 ms	19.3±1.4	250	2	[23,24]
25	2018/01/10 02:54:50	4	TF	770.4	9012±19	18	0.4–20	±1 μs	19.3±1.4	250	2	[23,24]
26	2018/01/10 02:57:56	3	S	699.1	24081±34	47	0.4–20	±1 s	19.3±1.4	250	2.2	
27	2018/01/10 07:34:56	1	A	9.3	419±31	103	0.4–24	±1 s	16.1±1.2	250	1.6	
28	2018/01/10 11:59:10	6	A	3.3	N/A	N/A	0.4–25	±1 μs	13.8±1.6	250	2.2	
29	2018/01/10 12:02:25	6	A	27.4	1168±21	48	0.4–25	±1 μs	13.8±1.6	250	2.2	
30	2018/01/11 10:40:13	6	A	34.0	1075±29	53	0.4–25	±1 μs	18.2±1.3	240	-0.4	
31	2018/01/13 12:01:01	8	S	13.3	368±21	40.5	0.4–26	±1 μs	10.8±1.5	260	1.2	
32	2018/01/13 12:01:04	7	S	15.2	511±24	53	0.4–27	±1 μs	10.8±1.5	260	1.2	
33	2018/01/23 13:29:06	2	S	5.7	265±36	84	0.4–23	±1 μs	25.6±1.3	250	3.2	
34	2018/02/04 03:50:31	6	S	8.2	226±36	97	0.4–24	±1 μs	13.8±1.5	250	1.1	
35	2018/12/08 20:53:18	5	S	5.1	152±36	46	0.4–23	±1 μs	14±1.3	250	5.1	
36	2018/12/08 21:09:21	3	S	13.2	776±33	93.5	0.4–20	±1 s	14±1.3	250	5.5	
37	2018/12/08 21:10:57	4	S	6.7	503±42	161.5	0.4–21	±1 μs	14±1.3	250	5.5	
38	2018/12/17 18:51:30	10	T	3.9	N/A	N/A	0.4–22	±1 μs	10.9±1.3	270	7.7	
39	2018/12/17 18:54:11	9	T	9.1	95±11	12	0.4–18	±1 μs	10.9±1.3	270	7.7	
40	2018/12/17 18:54:11	10	T	13.6	273±15	23.5	0.4–22	±1 μs	10.9±1.3	270	7.7	
41	2018/12/17 19:15:03	10	S	7.4	383±28	69	0.4–22	±1 μs	10.6±1.2	270	5.9	
42	2018/12/17 19:15:16	9	S	18.2	678±24	51.5	0.4–18	±1 μs	10.6±1.2	270	5.9	
43	2018/12/17 23:15:34	3	S	20.6	1024±29	63	0.4–20	±1 s	11.3±1.3	280	8.4	

TABLE II. (*Continued.*)

No.	Detection time (JST)	Site	Type <sup>a</sup>	Signif. <sup>b</sup>	Num. of photons	Duration (s)	Energy range (MeV)	Timing accuracy	Wind <sup>c</sup>		Temp. (°C)	Pub. <sup>d</sup>
									speed (m s <sup>-1</sup> )	direction (degree)		
44	2018/12/17 23:17:04	4	S	24.3	1399±33	89.5	0.4–22	±1 μs	11.3±1.3	280	8.4	
45	2018/12/18 23:40:06	8	T	6.8	86±13	15.5	0.4–24	±1 μs	13.5±1.3	270	8.1	
46	2018/12/18 23:42:05	8	S	53.6	2117±27	56.5	0.4–24	±1 μs	13.5±1.3	270	8.1	
47	2018/12/18 23:42:56	9	T	38.2	515±16	25.5	0.4–18	±1 μs	13.5±1.3	270	8.1	
48	2018/12/18 23:42:56	10	T	9.8	131±17	26.5	0.4–22	±1 μs	13.5±1.3	270	8.1	
49	2018/12/18 23:49:40	5	T	10.5	147±14	17	0.4–24	±1 μs	11.9±1	270	6.6	[21]
50	2018/12/18 23:51:48	5	T	311.0	7351±23	32	0.4–24	±1 μs	11.9±1	270	6.6	[21]
51	2019/01/22 00:51:33	8	T	11.9	331±19	31	0.4–24	±1 μs	14.2±1.2	280	5.6	
52	2019/01/22 01:03:48	5	A	38.5	1678±35	69	0.4–23	±1 μs	13.6±1.1	270	4.2	[21]
53	2019/01/25 20:43:43	6	S	10.6	293±25	39.5	0.4–25	±1 μs	16.9±1.2	260	2.8	
54	2019/01/25 20:44:30	8	S	8.2	324±28	51	0.4–24	±1 μs	16.9±1.2	260	2.8	
55	2020/01/13 02:03:23	3	T	70.0	1034±18	19.5	0.4–20	±1 μs	16.4±1.4	240	6.2	[25]
56	2020/01/13 02:03:23	4	T	32.7	354±20	14	0.5–22	<1 ms	16.4±1.4	240	6.2	[25]
57	2020/01/13 02:05:35	3	A	131.4	3339±29	34	0.4–20	±1 μs	16.4±1.4	240	6.2	[25]
58	2020/01/13 02:06:59	4	TF	111.9	5316±32	59	0.5–22	<1 ms	16.4±1.4	240	6.2	[25]
59	2020/02/17 20:52:56	11	TF	7.8	112±17	27	0.7–15	±1 μs	15.7±1.2	260	2.5	
60	2020/02/17 21:00:14	5	A	61.6	3605±44	111	0.4–23	±1 μs	15.7±1.2	260	2.4	
61	2020/02/17 21:47:11	11	A	3.9	N/A	N/A	0.7–15	±1 μs	15±1.2	250	2.6	
62	2020/02/17 21:49:40	3	S	10.3	501±26	63	0.4–20	±1 μs	15±1.2	250	2.6	
63	2020/02/17 21:49:46	11	A	9.4	634±32	86	0.7–15	±1 μs	15±1.2	250	2.6	
64	2020/02/17 21:51:17	4	S	10.9	805±29	73	0.5–20	±1 μs	15±1.2	250	2.6	
65	2020/02/17 21:52:17	3	A	84.2	3958±35	86	0.4–20	±1 μs	15±1.2	250	2.6	
66	2020/02/17 21:53:54	4	A	99.1	4023±32	49.5	0.5–20	±1 μs	15±1.2	250	2.6	
67	2020/02/18 01:29:17	10	A	86.3	4771±33	89.5	0.3–15	±1 μs	12.7±1.3	260	1.1	
68	2020/02/18 01:30:42	9	T	60.2	3491±31	110.5	0.4–17	±1 μs	12.7±1.3	260	1.1	
69	2020/02/18 01:35:23	2	A	87.0	5355±41	120	0.4–22	±1 μs	13.6±1.3	260	1.9	
70	2020/03/16 06:28:10	5	T	41.2	1722±26	58	0.4–23	±1 μs	13±1.2	280	4.1	

<sup>a</sup>S, A, and T mean a gamma-ray glow with temporarily symmetric count-rate variation, with temporarily asymmetric count-rate variation, and a glow terminated with a lightning discharge, respectively. TF means a glow terminated with a downward TGF besides a lightning discharge.

<sup>b</sup>The significance of each event calculated for the event scan.

<sup>c</sup>The wind direction is where the wind comes from in clockwise. See the main text.

<sup>d</sup>Publication references if it is a previously published event.

(Bi<sub>4</sub>Ge<sub>3</sub>O<sub>12</sub>) or a 30.0 × 5.0 × 5.0 cm<sup>3</sup> cesium iodide (CsI) crystal. While the BGO crystal is coupled with two Hamamatsu R1924A photomultipliers, the CsI crystal is coupled with a Hamamatsu R6231 photomultiplier. Signals from the photomultipliers are amplified via a preamplifier and a shaping amplifier, then digitally sampled by an analog-to-digital convertor. Information of gamma rays, including energy and detection timing, is stored by Raspberry Pi. Details of the detection system are described in Ref. [22]. The energy range of the radiation monitors varies because configurations (high voltage and lower threshold) can be changed in each year, but a typical range is 0.4–20.0 MeV.

The absolute timing is conditioned by global positioning system (GPS) signals. When GPS signals are successfully received, the absolute timing accuracy is ±1 μs. When signals

are temporarily lost (during up to several hours), we interpolate the absolute timing with the GPS signals received before and after the loss. In this case, the precision is better than 1 ms. When GPS signals are completely lost, the absolute timing is assigned by the internal clock of Raspberry Pi, conditioned by the network timing protocol (NTP) service. This case provides a timing precision of 1 s. If neither the GPS signal nor the Internet connection is lost, we still rely on the internal clock of Raspberry Pi, but the absolute timing accuracy is unknown. In FY2016, due to a hardware issue, the absolute accuracy is ±0.5 s even when GPS signals are successfully received. This accuracy can be improved by further individual calibration as reported in Ref. [6], but we retain this accuracy in the present paper because this catalog analysis does not require more precision. Throughout this paper, we use Japan

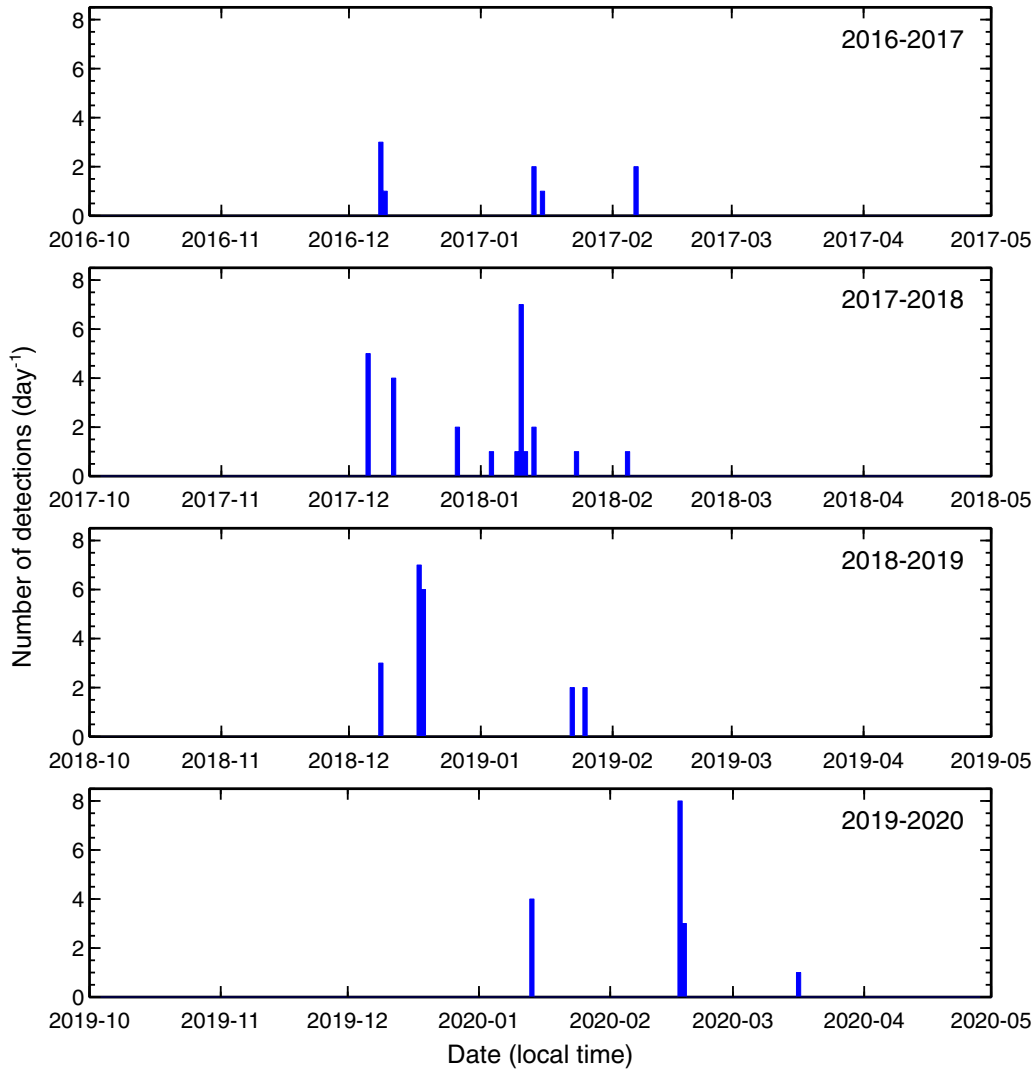


FIG. 3. Time histories of the number of gamma-ray glow detections per day.

Standard Time (JST: UTC+9) to associate gamma-ray glows with daily variations of meteorological conditions in the local time.

### III. RESULTS

#### A. Event detection

Gamma-ray glows can be identified as count-rate enhancements from background levels. The event scan was made using the method introduced in Ref. [22]. First, count-rate histories with 10-s bins are produced. We employ the energy range above 3 MeV because this range is not affected by radon-decay-chain background variations. With the 10-s-binned count-rate histories, the standard deviation and the mean count rate are computed every 30 min. Then the significance of each bin is calculated; the count rate is divided by the standard deviation after the mean count rate is subtracted. If the significance of a bin exceeds 5 standard deviations ( $5\sigma$ ), it is considered as a potential glow event. Finally, glow events are added to our event list by checking the count-rate histories manually. In this method, fainter events with a significance of less than  $5\sigma$  are usually ignored. On the other hand, glows

with a significance of less than  $5\sigma$  can be coincidentally identified when searching over the data around the automatically detected events. Such fainter glows are also added to the present event list. Most of the events were detected on thunder days in Kanazawa, confirmed by reports of the Japan Meteorological Agency. The others were confirmed by meteorological radar to coincide with the passage of a strong radar echo above the gamma-ray detector,

During the four winter seasons, a total of 70 gamma-ray glows were detected. The event list is shown in Table II. Among the 70 gamma-ray glows, 66 have a significance of more than  $5\sigma$ , and the remaining 4 glows have less significance. Twenty-four events have been reported in our previous publications [21–25]. There are simultaneous detections with nearby detectors (Events 2 and 3, for example). They can be interpreted as an identical gamma-ray glow that passed over multiple radiation detectors with ambient wind flow [22,24]. In the present paper, however, we consider a gamma-ray enhancement recorded by a radiation detector as an event in order to avoid interpretations in the event list.

Figure 3 shows the number of detected glows per day. The largest number of gamma-ray glows was detected on 17

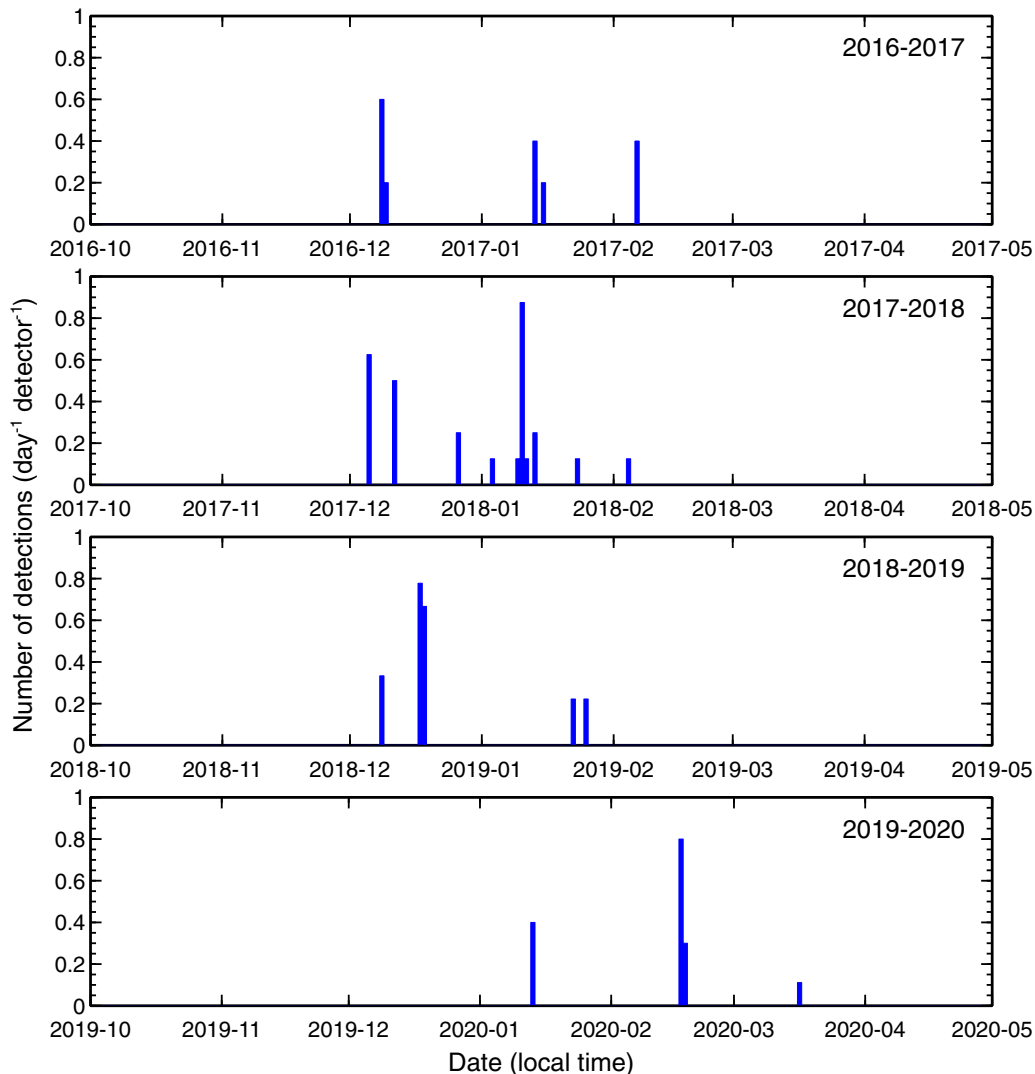


FIG. 4. Time histories of the number of gamma-ray glow detections per -day, normalized by the number of radiation detectors in operation.

February 2020 (8 events). The second largest number is 7 events on 10 January 2018 and 17 December 2018. However, these data do not indicate the occurrence rates of gamma-ray glows because the number of deployed detectors differs, as shown in Fig. 2. Figure 4 presents the same data as in Fig. 3 but normalized by the number of radiation detectors in operation, as shown in Fig. 2. On 10 January 2018, 8 detectors were in operation and 7 events were detected. Hence on average 0.88 events were detected by a detector in the day. Nearly one event can be detected by one detector on days under heavy thunderstorms. The first peak of events typically comes in the beginning or middle of December. In addition, there is sometimes a second peak in the middle of January.

The monthly variation of glow detections is shown in Fig. 5. The upper panel presents accumulated data for four seasons. The largest number of glows was detected in December, while no events were detected in October and November. These data should also be normalized by the number of detectors in operation, as in the lower panel of Fig. 5. December still has the largest number of glows, and most of the events were detected during December–February. On average, every detector registered nearly one event in December. Though the

detectors continue observation, glow events in March are quite rare (only Event 70 on 16 March 2020). A detailed discussion is given in Sec. IV.

In addition, the yearly variation of event detections is shown in Fig. 6. In FY2017 (the 2017–2018 season), the largest number of events (25 glows) was detected. This trend is still true even after being normalized by the number of deployed detectors as in the lower panel. FY2017 was the most significant season for glow observations in four years; on average, 3–4 events were detected by a detector during the season. The detection rates in the other three seasons were similar, i.e., 1–2 events by a detector during a season on average.

The hourly variation of event detections is shown in Fig. 7. The largest number of events was detected during 02:00–03:00 JST. Also during 21:00–22:00 and 23:00–24:00 JST the second largest number of gamma-ray glows was registered. While 23% of events were detected during 06:00–18:00, 77% were during 18:00–24:00 and 00:00–06:00. Therefore, nighttime tends to have more opportunities to detect gamma-ray glows than daytime.

The variations in the number of events by observation sites are shown in Fig. 8. As mentioned in Ref. [21], the largest

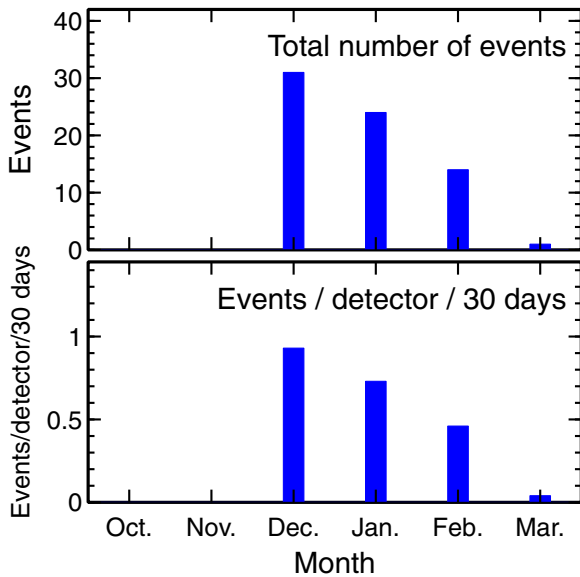


FIG. 5. Monthly variations in the accumulated number of glow events. The upper panel shows the raw histogram, and the lower shows the data normalized by the number of detectors in operation, thus indicating the averaged number of event detections by a radiation monitor in a month.

number of gamma-ray glows was detected at site 5, Kanazawa University Kakuma Campus, i.e., 15 events for four years. The lower panel shows the normalized distribution by operational days. The highest frequency of event detections is at site 10 (3.68 events/120 days). This site was operated in FY2018 and FY2019, but its operation was accidentally suspended in January in FY2019. Therefore, the frequency is high for site 10 even though the total number of detections is only 5.

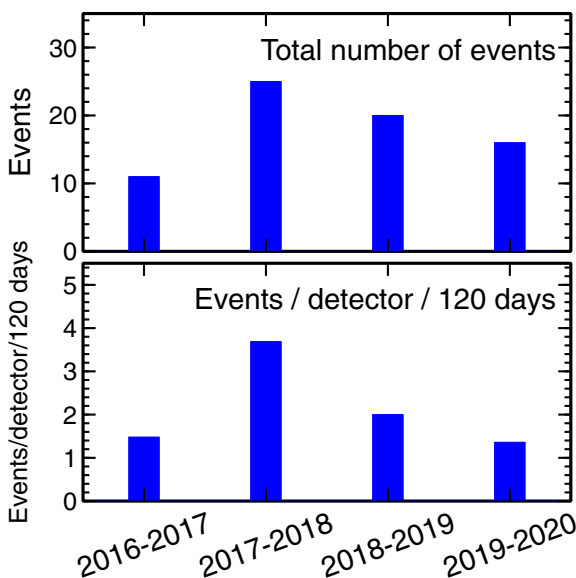


FIG. 6. Yearly variations in the accumulated number of glow events. The upper panel shows the raw histogram, and the lower shows the data normalized by the number of detectors in operation, thus indicating the averaged number of event detections by a radiation monitor in a winter season. Here a winter observation period is considered to continue for 120 days (4 months) on average.

### B. Temporal analysis

This subsection presents temporal analyses of individual events based on count-rate histories. Count-rate histories of all 70 events are shown in Appendix. First of all, the gamma-ray glows can apparently be classified into three types based on the shape of the histories: temporally symmetric with a single peak, temporally asymmetric with single or multiple peaks, and lightning-terminated. The classification is included in Table II. Among the 70 detected glows, 34 events are the temporally symmetric type, 17 are temporally asymmetric, and the remaining 19 events are terminated with lightning discharges.

The temporally asymmetric type might be further divided into two types: single-peak and multiple-peak. Clear examples of the multiple-peak type are Events 22 and 52. We can easily identify two peaks in an event. On the other hand, the boundary between the two types is vague. For example, Event 29 seems to have two peaks, but they are not well separated and hence they can also be considered as a single-peaked asymmetric type.

The lightning-terminated type has a sudden decrease in count rates. For most of the termination events except Event 38, the Japanese Lightning Detection Network (JLDN) reported one or multiple nearby lightning currents within 10 km from the observation sites at the moment of termination, detected by a low-frequency measurement. Furthermore, the termination of Events 25, 58, and 59 coincided with a downward TGF. Events 25 and 58 were reported in Refs. [24] and [25], respectively. The other cases coincided with no downward TGFs.

To examine the brightness of the gamma-ray glows, the number of detected photons is calculated. To eliminate the background variations by a radon-decay chain, here again signals above 3 MeV are counted. The method to constrain the number of photons is as follows: first a source window that covers the entire event is set, and photons above 3 MeV in the windows are counted. Next, another window that has the same duration as the source window is set to a background period, and photons above 3 MeV in the windows are also counted. The background period of each event is described in the public materials (see the Acknowledgments). Then, the number of photons in the background window is subtracted from that in the source window. The uncertainty of this method is the difference in the photons in the background window and the actual background photons in the source window. Therefore, we consider the Poisson error of the photon number in the background window as the error of this estimation. This calculation is applied to the glows with  $>5\sigma$  detection significance. For the glows terminated with a downward TGF, photons after the TGFs are not included to properly evaluate the gamma-ray glows.

The results are shown in Table II and Fig. 9. Due to the differences in detector responses/effective areas of the BGO and CsI crystals, the results are displayed separately. The largest number is 24 081 photons and 4771 photons for detectors with BGO and CsI crystals, respectively. The geometric mean is 1105 photons and 458 photons, and the median is 1024 photons and 383 photons, respectively.

Another key parameter is duration. Here we define T80 duration: the duration window starts when the accumulated photon number exceeds 10% of the total detected photon

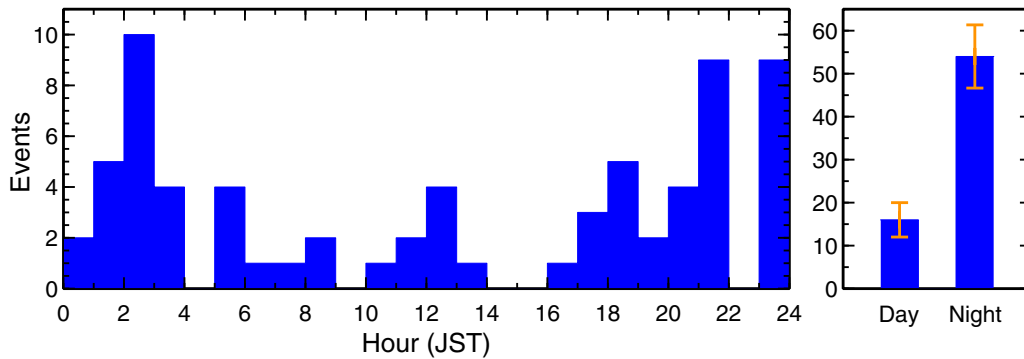


FIG. 7. Hourly variation in the accumulated number of glow events (left) and the difference in the number of detections (right) during daytime (06:00–18:00 JST) and nighttime (00:00–06:00 and 18:00–23:00 JST). The orange bars in the right panel indicate one standard deviation of the Poisson distribution.

number calculated above, and it ends when the accumulated number exceeds 90% of the total photon number. A similar method, T90, is often used for gamma-ray bursts in astrophysics [56]. The calculation was executed with 0.5-s steps to consider deadtime correction. The results are listed in Table II and also displayed in Fig. 9. In addition to the photon number, this calculation is applied to the glows with  $>5\sigma$  detection significance, and the results from the BGO and CsI crystals are separated. The longest duration is 161.5 and 110.5 s for detectors with BGO and CsI crystals, respectively. The average duration is 63.2 and 49.7 s, and the median is 56.0 and 48.0 s, respectively. When the results of BGO and CsI crystals are combined, the average duration is 58.9 s.

In addition to the calculation of the photon number and duration, we test a function fitting of the count-rate histories. Since the count-rate histories, in particular the temporally symmetric type, may be approximated by a Gaussian function, Gaussian fitting to the histories is examined. The fitting function  $F(t)$  is

$$F(t) = C_{\text{bgd}} + \sum_{i=1}^n a_i \exp \left\{ -\frac{(t - T_i)^2}{2\sigma_i^2} \right\}, \quad (1)$$

where  $t$  is time,  $C_{\text{bgd}}$  is a constant value of the background count rate,  $a$  is the peak count rate,  $T$  is the peak time,  $\sigma_i$  is the standard deviation of the Gaussian function, and  $n$  is the number of Gaussian functions to be added.  $n$  should be as small as possible. In most cases of the temporally symmetric type, one Gaussian function can reproduce the count-rate histories, and hence  $n = 1$ . On the other hand,  $n$  can be more than 1 for a part of the temporally symmetric type that cannot be approximated by a Gaussian function, and for the temporally asymmetric type. This fitting is also applied to a part of the lightning-terminated type if the events have a count-rate peak before the termination. In this case, a step function is folded to Eq. (1) to imitate the termination. The moment of termination is set to be that of the lightning discharge reported by JLDN. It is noted that there is no physical reason to utilize the Gaussian function, but this is a tentative attempt to evaluate the shape of the count-rate histories.

The fitting results are overlaid in Figs. 17–23. Most of the symmetric-type events and a part of lightning-terminated events can be approximated by a single Gaussian function plus a background constant. A symmetric-type event (Event 26) and most of the asymmetric-type events can be

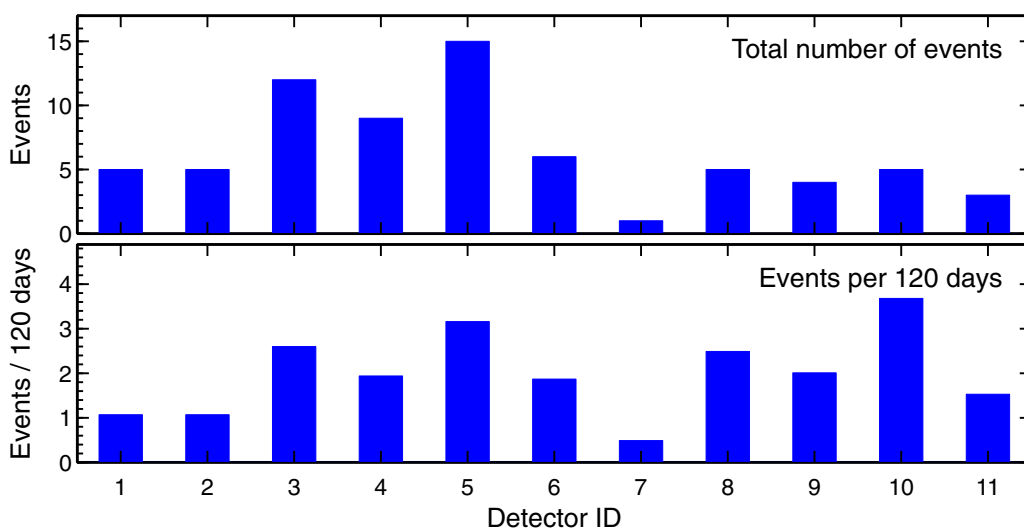


FIG. 8. The total number of detections (upper) and the normalized one (lower) for each observation site. The lower panel shows the detection frequency in a 4-month period, a typical observation period in a winter season.

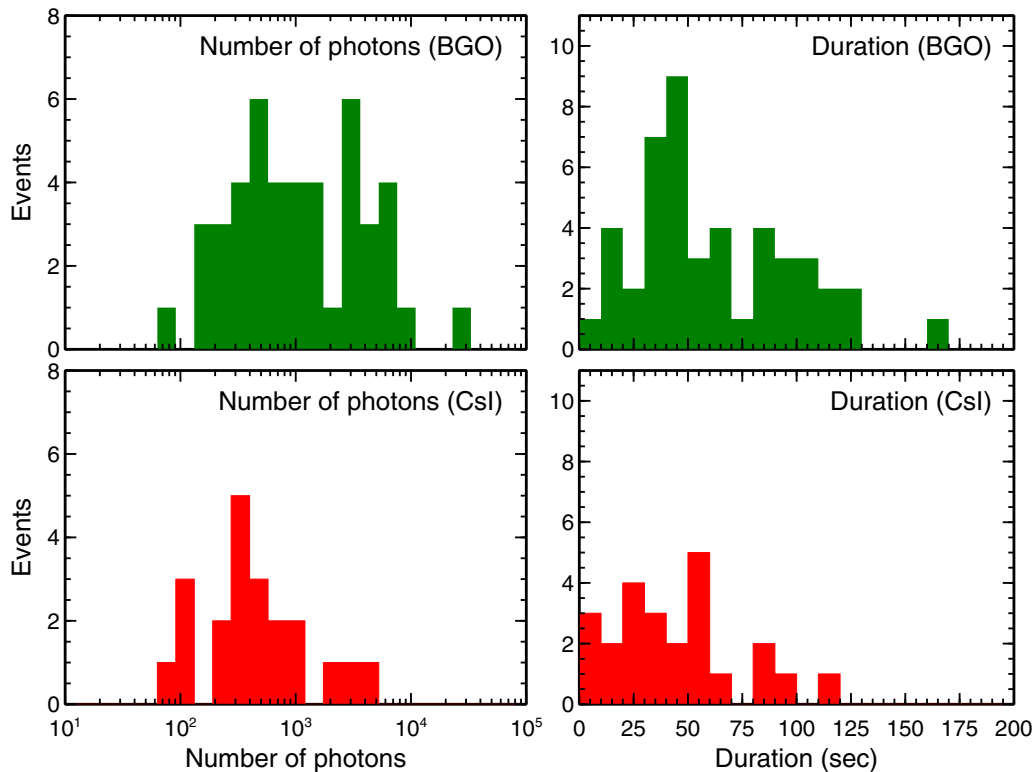


FIG. 9. Histograms of the detected photon numbers (left) and the duration of gamma-ray glows registered with the BGO (upper) and CsI (lower) crystals.

approximated by two Gaussian functions plus a constant. Events 22 and 60 require three Gaussian components. The moment of termination in Event 15 is different from that reported by JLDN. Because the radiation monitor in Site 3 lost both GPS signals and the Internet connection at that moment, the absolute timing is unreliable, the discrepancy is not solid, and thus we ignore it.

### C. Spectral analysis

Next we examine the spectral analysis of the gamma-ray glows. The analysis is performed with XSPEC, a spectral analysis framework for high-energy astrophysics [57]. XSPEC can unfold detector responses when an appropriate fitting function and the response matrix are given to derive the incident photon fluxes. The response matrices for the BGO and CsI scintillators were produced by Monte Carlo simulations with the simulation framework GEANT4 [58–60], as shown in Ref. [22]. Among the 70 events, we focus on 28 events with >1000 photons above 3 MeV in order to avoid analyses with poor photon statistics. Also, a background spectrum is subtracted from the source spectrum. Background spectra can change below 3 MeV as this energy band is affected by the radon-decay chain emission. It can lead to a large systematic uncertainty of the background-subtracted spectra below 3 MeV if the intrinsic glow flux is low. Therefore, the spectral analysis is applied to the events with high photon statistics.

The source spectrum for each event is extracted from the T80 window, namely the window between two blue-dashed lines in Figs. 17–23 of Appendix. The window for the background spectrum is set to have the same duration as the source

window, not to include the gamma-ray glow, but to include a nearby background period. The background-subtracted spectra are fitted by a power-law function with an exponential cutoff  $S(E)$ ,

$$S(E) = A \times E^{-\Gamma} \exp\left(-\frac{E}{E_{\text{cut}}}\right), \quad (2)$$

where  $E$ ,  $A$ ,  $\Gamma$ , and  $E_{\text{cut}}$  are the energy of gamma-ray photons, the normalization factor, the power-law index, and the cutoff energy, respectively. This is an approximated form of a bremsstrahlung spectrum produced by RREA electrons [61]. The energy flux in 0.2–20.0 MeV  $F_{0.2-20}$  is derived as

$$F_{0.2-20} = \int_{0.2 \text{ MeV}}^{20 \text{ MeV}} A \times E^{-\Gamma} \exp\left(-\frac{E}{E_{\text{cut}}}\right) E dE \quad (3)$$

by extrapolating the gamma-ray spectrum down to 0.2 MeV with best-fit parameters. The fitting energy range varies by events because the energy range depends on detectors, due to differences in amplifier gain and lower and upper thresholds. The fitting is performed to cover the full energy range of each event, but it uses above 0.6 MeV for all the events because the range below 0.6 MeV can be affected by the annihilation line at 0.511 MeV and hence cannot be fitted only with the power-law function.

All the response-folded and response-unfolded spectra are shown in Figs. 24–29. The best-fit functions are also overlaid. The fitting parameters are listed in Table III. Histograms of the parameters are also shown in Fig. 10. The power-law index is 0.50 on average, with a standard deviation of 0.28. In addition, the average of the cutoff energy is 4.41 MeV,

TABLE III. The result of spectral fitting.

No.	Crystal	Index	Cutoff (MeV)	Flux <sup>a</sup> erg cm <sup>-2</sup> s <sup>-1</sup>	Fluence <sup>a</sup> erg cm <sup>-2</sup>
3	BGO	0.17 ± 0.08	3.9 <sup>+0.3</sup> <sub>-0.2</sub>	(4.62 ± 0.08) × 10 <sup>-6</sup>	(4.53 ± 0.08) × 10 <sup>-4</sup>
6	BGO	0.66 ± 0.04	3.96 <sup>+0.2</sup> <sub>-0.19</sub>	(1.94 ± 0.02) × 10 <sup>-5</sup>	(8.16 ± 0.1) × 10 <sup>-4</sup>
13	BGO	0.66 ± 0.06	4.3 ± 0.3	(8.14 ± 0.15) × 10 <sup>-6</sup>	(3.58 ± 0.06) × 10 <sup>-4</sup>
14	BGO	0.62 <sup>+0.14</sup> <sub>-0.15</sub>	4.2 <sup>+0.7</sup> <sub>-0.6</sub>	(1.5 ± 0.06) × 10 <sup>-6</sup>	(1.62 ± 0.06) × 10 <sup>-4</sup>
16	BGO	0.91 <sup>+0.06</sup> <sub>-0.07</sub>	4.3 ± 0.4	(9.39 ± 0.18) × 10 <sup>-6</sup>	(2.4 ± 0.05) × 10 <sup>-4</sup>
19	BGO	0.19 ± 0.06	4.3 ± 0.2	(1.26 ± 0.02) × 10 <sup>-5</sup>	(4.35 ± 0.07) × 10 <sup>-4</sup>
20	BGO	0.43 ± 0.05	4.8 ± 0.2	(1.13 ± 0.018) × 10 <sup>-5</sup>	(4.41 ± 0.07) × 10 <sup>-4</sup>
22	BGO	0.39 ± 0.04	3.98 ± 0.14	(9.84 ± 0.11) × 10 <sup>-6</sup>	(9.06 ± 0.1) × 10 <sup>-4</sup>
24	BGO	0.81 ± 0.04	4.7 ± 0.2	(1.61 ± 0.02) × 10 <sup>-5</sup>	(5.71 ± 0.07) × 10 <sup>-4</sup>
25	BGO	0.74 ± 0.02	4.84 ± 0.13	(7.42 ± 0.05) × 10 <sup>-5</sup>	(1.336 ± 0.01) × 10 <sup>-3</sup>
26	BGO	0.604 ± 0.013	4.43 ± 0.07	(8.15 ± 0.04) × 10 <sup>-5</sup>	(3.83 ± 0.017) × 10 <sup>-3</sup>
29	CsI	0.2 <sup>+0.13</sup> <sub>-0.15</sub>	3.2 ± 0.3	(4.46 ± 0.14) × 10 <sup>-6</sup>	(2.14 ± 0.06) × 10 <sup>-4</sup>
30	CsI	0.98 ± 0.1	4.8 <sup>+0.7</sup> <sub>-0.6</sub>	(4.47 ± 0.13) × 10 <sup>-6</sup>	(2.37 ± 0.07) × 10 <sup>-4</sup>
43	BGO	-0.1 ± 0.3	4.6 <sup>+0.9</sup> <sub>-0.7</sub>	(2.04 ± 0.09) × 10 <sup>-6</sup>	(1.28 ± 0.06) × 10 <sup>-4</sup>
44	BGO	-0.1 ± 0.2	3.9 <sup>+0.5</sup> <sub>-0.4</sub>	(1.94 ± 0.07) × 10 <sup>-6</sup>	(1.74 ± 0.06) × 10 <sup>-4</sup>
46	CsI	0.38 ± 0.09	4.3 ± 0.3	(6.43 ± 0.14) × 10 <sup>-6</sup>	(3.63 ± 0.08) × 10 <sup>-4</sup>
50	BGO	0.42 ± 0.03	4.52 ± 0.12	(3.15 ± 0.03) × 10 <sup>-5</sup>	(1.009 ± 0.009) × 10 <sup>-3</sup>
52	BGO	0.61 <sup>+0.08</sup> <sub>-0.09</sub>	4.9 <sup>+0.5</sup> <sub>-0.4</sub>	(3.65 ± 0.09) × 10 <sup>-6</sup>	(2.52 ± 0.06) × 10 <sup>-4</sup>
55	BGO	0.43 <sup>+0.1</sup> <sub>-0.11</sub>	4.6 <sup>+0.5</sup> <sub>-0.4</sub>	(7.3 ± 0.2) × 10 <sup>-6</sup>	(1.43 ± 0.04) × 10 <sup>-4</sup>
57	BGO	0.34 ± 0.05	4.26 <sup>+0.2</sup> <sub>-0.19</sub>	(1.35 ± 0.02) × 10 <sup>-5</sup>	(4.58 ± 0.07) × 10 <sup>-4</sup>
58	BGO	0.48 ± 0.04	4.79 <sup>+0.19</sup> <sub>-0.18</sub>	(1.263 ± 0.015) × 10 <sup>-5</sup>	(7.45 ± 0.09) × 10 <sup>-4</sup>
60	BGO	0.88 <sup>+0.04</sup> <sub>-0.05</sub>	4.7 ± 0.3	(5.35 ± 0.08) × 10 <sup>-6</sup>	(5.94 ± 0.09) × 10 <sup>-4</sup>
65	BGO	0.91 ± 0.04	4.6 ± 0.2	(7.67 ± 0.1) × 10 <sup>-6</sup>	(6.6 ± 0.08) × 10 <sup>-4</sup>
66	BGO	0.91 ± 0.04	5.1 ± 0.2	(1.317 ± 0.016) × 10 <sup>-5</sup>	(6.52 ± 0.08) × 10 <sup>-4</sup>
67	CsI	0.28 <sup>+0.06</sup> <sub>-0.07</sub>	4.4 ± 0.2	(9.02 ± 0.13) × 10 <sup>-6</sup>	(8.08 ± 0.12) × 10 <sup>-4</sup>
68	CsI	0.44 <sup>+0.07</sup> <sub>-0.08</sub>	4.4 ± 0.3	(5.58 ± 0.1) × 10 <sup>-6</sup>	(6.17 ± 0.11) × 10 <sup>-4</sup>
69	BGO	0.26 <sup>+0.05</sup> <sub>-0.06</sub>	4.7 ± 0.2	(5.82 ± 0.08) × 10 <sup>-6</sup>	(6.99 ± 0.1) × 10 <sup>-4</sup>
70	BGO	0.49 ± 0.09	3.8 ± 0.3	(4.23 ± 0.1) × 10 <sup>-6</sup>	(2.45 ± 0.06) × 10 <sup>-4</sup>
(average)	BGO	0.613 ± 0.009	4.68 ± 0.04	(1.013 ± 0.003) × 10 <sup>-5</sup>	

<sup>a</sup>The energy range is 0.2–20.0 MeV.

with a standard deviation of 0.41 MeV. The energy flux varies from  $1.5 \times 10^{-6}$  to  $8.1 \times 10^{-5}$  erg cm<sup>-2</sup> s<sup>-1</sup>, with a geometric mean of  $8.4 \times 10^{-6}$  erg cm<sup>-2</sup> s<sup>-1</sup>. Scatter plots between two parameters of three are shown in Fig. 11. There are no significant correlations between the energy flux and the power-law index nor between the energy flux and the cutoff energy. This feature is different from observations in Aragats [53], which report a clear positive correlation between the power-law index and intensity at 1 MeV. The power-law index and the cutoff energy have a moderate negative correlation with a correlation coefficient of 0.47.

We then extract an averaged spectrum to derive typical parameters of glow spectra. Here the energy spectra of 21 glows detected by the BGO crystals are accumulated because the spectra of BGO and CsI crystals cannot be summed up due to the difference in detector responses. Also, Events 3 and 6 were excluded from this analysis because the energy range of these events is narrower than that of the others, and

hence they would reduce the quality of the analysis. The fitting range is set to 0.5–20.0 MeV. For spectral fitting, a Gaussian function is added to the power-law function in order to reproduce the annihilation line at 0.511 MeV. The total exposure is 1234.0 s. The averaged spectrum and the fitting result are shown in Fig. 12. The reduced  $\chi^2$  of the best-fit function is 2.3 with 46 degrees of freedom. Even after unfolding the detector responses, the exponential roll-off can be clearly seen around 5 MeV. The power-law index, cutoff energy, and energy flux of the best-fit function are  $0.613 \pm 0.009$  MeV,  $4.68 \pm 0.04$  MeV, and  $(1.013 \pm 0.003) \times 10^{-5}$  erg cm<sup>-2</sup> s<sup>-1</sup> (0.2–20.0 MeV), respectively. The annihilation line has an equivalent width of  $38.8^{+1.7}_{-2.5}$  keV.

#### D. Meteorological conditions

Meteorological conditions, including ambient wind and atmospheric temperature, are of great interest for investigation

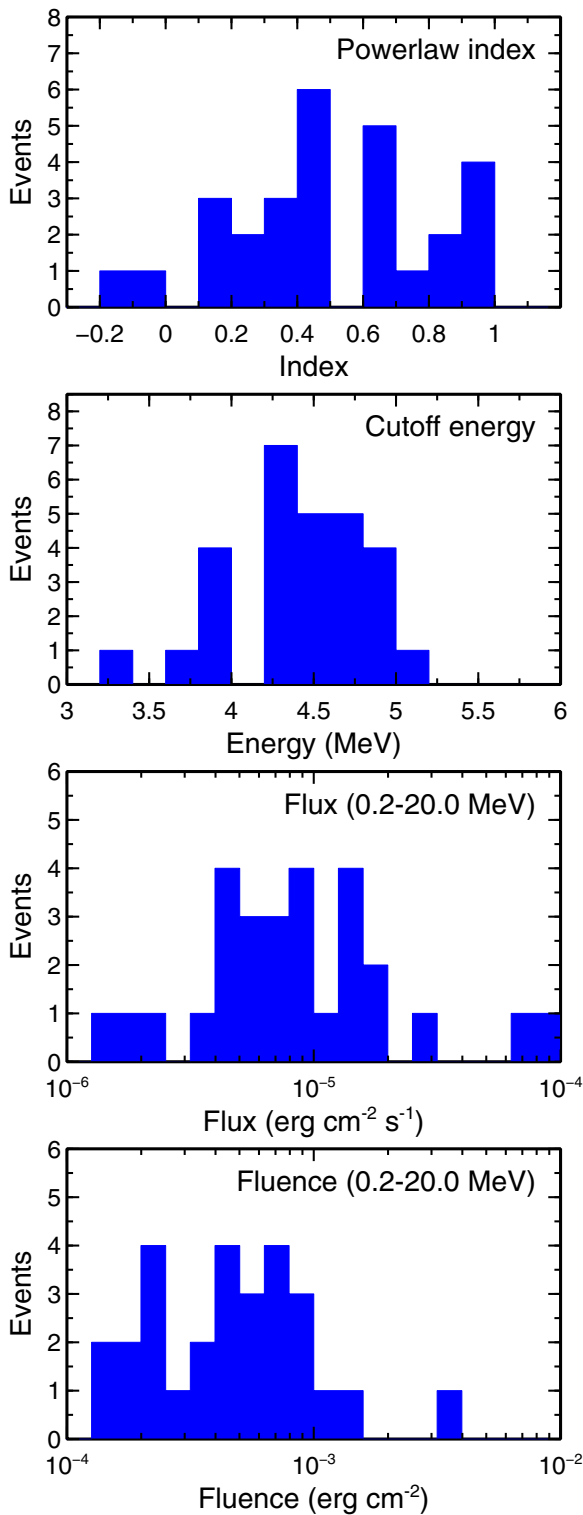


FIG. 10. Histograms of fitting parameters obtained by spectral analysis.

of gamma-ray glows. The wind speed and its direction at the moment of glow detections can be derived from meteorological radar data by calculating the moving vector with two time-separated radar contours. The detailed method of the calculation is introduced in Ref. [24]. This method works under the assumption that a cloud or an echo region moves

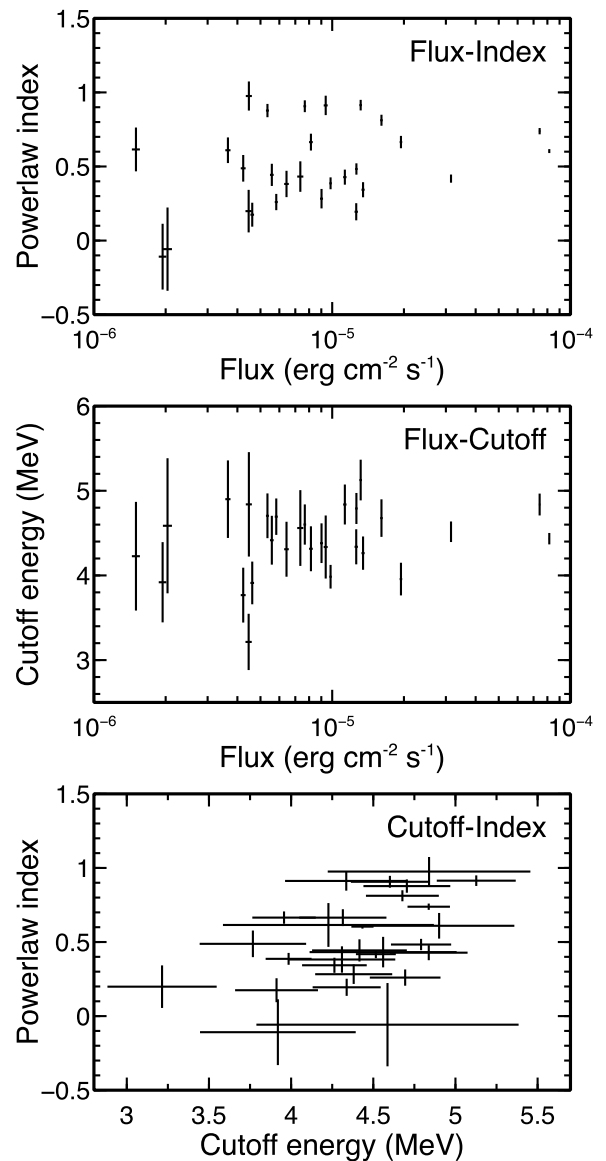


FIG. 11. Scatter plots of power-law index vs energy flux (upper), cutoff energy vs energy flux (middle), and power-law index vs cutoff energy (lower).

with ambient wind. We utilize the data of the eXtended RADar Information Network (XRAIN), operated by the Ministry of Land, Infrastructure, Transport and Tourism of Japan. Both the Komatsu and Kanazawa areas are covered by X-band (9.8 GHz) dual-polarized radar at the Noumi radar site of XRAIN. Synthetic precipitation contours or plan-position indicator contours of reflectivity factor obtained every minute are used for the wind estimation.

The estimated wind velocity and direction are listed in Table II. In addition, their histograms are shown in Fig. 13. The direction is where the wind comes in clockwise. For example, a direction of 270° means the wind comes from west to east. The average velocity is 15.3 m s<sup>-1</sup> with a standard deviation of 3.5 m s<sup>-1</sup>, and the average direction is 260° with a standard deviation of 15°. Most of the gamma-ray glows occurred during west or west-southwest winds, and a

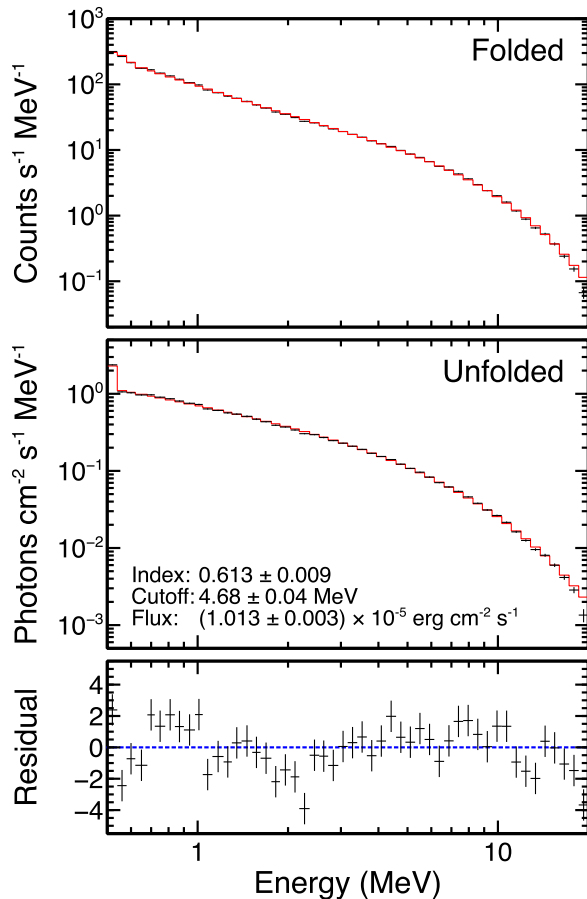


FIG. 12. The averaged energy spectrum of gamma-ray glows detected by the BGO scintillators. The red lines show the best-fit function. Upper: the energy spectrum in which the detector responses are included. Middle: the spectrum whose detector responses are unfolded by XSPEC (i.e., the incident flux right before reaching the detector). Lower: the fitting residual; each data point of the spectrum is divided by its statistical error after the corresponding model value is subtracted.

few during west-northwest winds. Gamma-ray glows never occurred during north, south, or east winds.

Atmospheric temperature during glows and its histogram are also presented in Table II and Fig. 14, respectively. The temperature was measured at Komatsu AMeDAS Station (N36.382°, E136.436°; for the events at sites 1 and 2) and Kanazawa Meteorological Observatory (N36.589°, E136.634°; for the other events) of the Japan Meteorological Agency. The histories of the temperature measurements can be retrieved from the website of the Japan Meteorological Agency. The average temperature is 4.6 °C with a standard deviation of 2.4 °C. Most cases occurred at a temperature above 0 °C, but two cases occurred below 0 °C (Events 7 and 30).

#### IV. DISCUSSION

Almost all the glows were detected from December to February, except for one event in March 2020. The detection frequency is the highest in December, as shown in the lower panel of Fig. 5. Winter thunderstorms in the Hokuriku region

usually start at the end of November or the beginning of December, and they end at the beginning of March. According to the records from the Japan Meteorological Agency, the average number of thunder days in Kanazawa during the four winter seasons (FY2016–FY2019) are 2.3, 5.5, 6.0, 3.0, and 2.8 days in November, December, January, February, and March, respectively. Therefore, the monthly variation of glow detections corresponds roughly to that of thunder days, even though the relation between them is not necessarily proportional. The number of thunder days in December–February are 17, 18, 10, and 10 days in FY2016, FY2017, FY2018, and FY2019, respectively. It is also consistent that FY2017, in which the highest number of glows were detected, had the highest number of thunder days. We note that during 1981–2020, the averaged number of thunder days in three months from December to February are 21.1 days (according to the Japan Meteorological Agency), significantly higher than in the four recent years presented here.

As in the Introduction, a typical cloud base of winter thunderclouds is several hundred meters, significantly lower than summer thunderclouds, and a typical cloud-top altitude is 5–6 km [6,21,30]. Since the charge center is close to the ground, gamma rays can reach detectors at sea level before they are attenuated in the atmosphere. The average temperature at the moment of glow detection is 4.6 °C, with a standard deviation of 2.4 °C, which is significantly lower than that when summer thunderstorms occur. In addition, a westerly wind is predominant in most cases. In the Hokuriku region, including Kanazawa and Komatsu, the north wind typically causes cold air to flow in, the surface temperature drops below freezing, and snowfall occurs. At that time, since the altitude at 0 °C where charging occurs reaches the ground, lightning does not occur in many cases, with some exceptions. Maintaining a surface temperature of around 5 °C with the westerly wind is a typical meteorological condition for gamma-ray glow. Further study of winter thunderstorms is needed in order to determine whether the conditions under which they occur are the same as those under which gamma-ray glows occur.

As described in Sec. III, the majority of gamma-ray glows have a symmetric count-rate history that can be approximated by one Gaussian function. This suggests that the irradiation area has a circle or ellipse shape, and it passes above a radiation detector with a constant wind flow. A schematic of this idea is shown in Fig. 15. In fact, Events 2 and 3 can be explained by the passage of a thundercloud, as presented in Ref. [22]. For the temporally asymmetric type, there are several interpretations. One is that multiple electron-acceleration regions adjoin each other, as in Fig. 15. This idea is supported by the result that temporally asymmetric glows are approximated by two or three Gaussian functions. In fact, several temporally asymmetric glows have two clear peaks (Events 22, 52, and 60), and they can be explained by this idea. Another interpretation is that the irradiation area does not have a circle or ellipse shape, but rather a more complex shape. This can occur when an electron-acceleration region has a complex shape or a tilt. It is also possible that an avalanche region rapidly glows and decays [25,62]. It is difficult to distinguish these ideas for the temporally asymmetric type with a single peak. As mentioned before, using Gaussian functions is tentative and empirical just to evaluate the shape of the gamma-ray

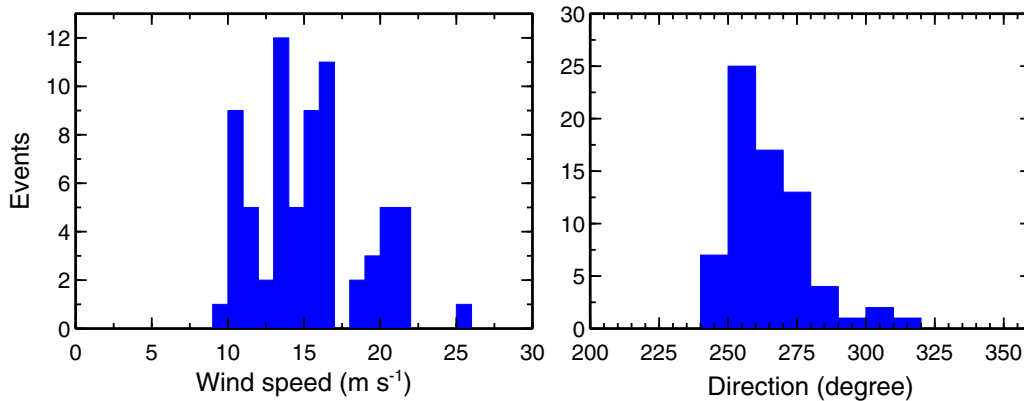


FIG. 13. Histograms of wind speed and its direction at the moment of glow detections. The direction is where the wind comes in clockwise. For example, a direction of  $270^\circ$  means the wind comes from west to east.

glows without enough physical reasoning. Therefore, some temporally asymmetric events could be explained and evaluated by other functions.

The spectral fittings allow us to reconfirm that the energy spectra of gamma-ray glows with high photon statistics can be approximated by the power-law function with an exponential cutoff, and hence can be explained by bremsstrahlung emission from electrons. The average cutoff energy, 4.41 MeV with a standard deviation of 0.41 MeV, is close to the average energy of RREA electrons ( $\sim 7.3$  MeV [61]). As in Fig. 3 of Dwyer *et al.* [61], the average energy of RREA electrons with an electric field below  $0.5 \text{ MV m}^{-1}$  can be lower than 7.3 MeV. Since gamma-ray glows are considered to occur in an electric field close to the RREA threshold, being different from TGFs, the obtained cutoff energy might reflect the electric field strength inside thunderclouds. However, the spectral shape is also affected by atmospheric scattering and absorption, and hence we need further investigations considering atmospheric propagation of gamma rays with Monte Carlo simulations.

As seen in the lower panel of Fig. 11, there is a positive correlation between the power-law index and the cutoff energy. However, these two parameters are not independent. Figure 16 shows a confidence area at one standard deviation in the space

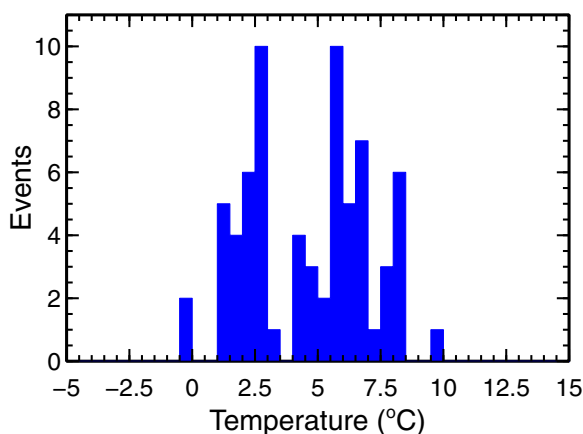


FIG. 14. A histogram of atmospheric temperature during gamma-ray glows, measured by the Japan Meteorological Agency.

of the power-law index and the cutoff energy, derived from the averaged energy spectrum. As the confidence area is a narrow ellipse, the parameters are coupled. This means that a function with a larger index and a larger cutoff energy is similar to that with a smaller index and a smaller cutoff energy. Therefore, this positive correlation is caused by the characteristics of the fitting function, and it does not necessarily have a physical meaning.

Chilingarian *et al.* [9] published a catalog of gamma-ray glows/TGEs detected at Mt. Aragats in Armenia in 2017. It is valuable to compare it with the present work. In 2017, 44 TGEs with high-energy particles (above 3 MeV) were detected at the Aragats Space Environment Center (ASEC). One of the significant differences is the seasons. They are all connected to summer thunderstorms from April to November, while our cases were during winter thunderstorms. Since ASEC is located at an altitude of 3200 m, a typical temperature at the moment of TGE detections ranges from  $-3$  to  $3^\circ\text{C}$  even in summer, which is lower than the average temperature of our cases.

Another significant difference is the number of detections: 44 TGEs from April to November, and hence 8.8 TGEs per month at a single site in their case. In the present analysis, the detection frequency is as many as 0.93 events per month per observation site. Therefore, TGEs/gamma-ray glows were detected more frequently at ASEC than in the Hokuriku region. This is potentially caused by the difference in meteorological conditions, namely the frequency of lightning discharges at Aragats and Hokuriku. Besides that, there is also a difference in atmospheric temperature. At ASEC, TGEs were detected frequently even below  $0^\circ$ . In these cases, the cloud base can get closer to the ground, and it is possible that sometimes the detectors are inside thunderclouds. This indicates that the detectors at ASEC are often closer to the acceleration region than in our cases, and they could have more opportunities to detect TGEs due to less atmospheric absorption of gamma rays.

## V. CONCLUSION

The mapping observation campaign, with up to 10 radiation monitors for four winter seasons, enabled us to observe

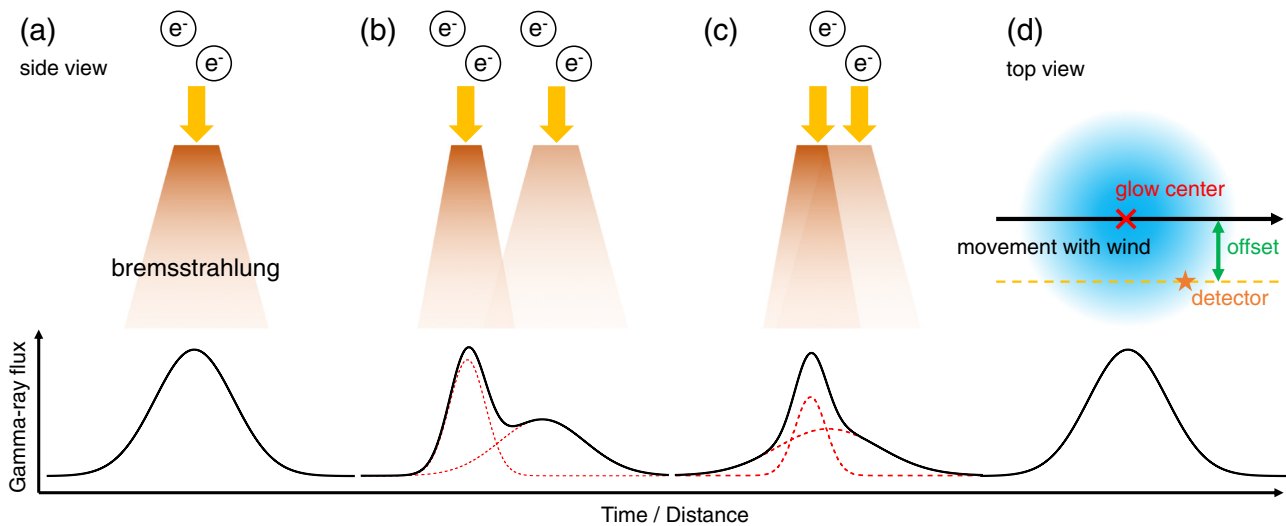


FIG. 15. Side-viewed schematics of the temporally symmetric (a), double-peaked (b), and temporally asymmetric (c) types, and a top-viewed relation between a temporally symmetric glow and a radiation detector (d). The blue region in panel (d) shows the radiation area of a gamma-ray glow on the ground.

70 gamma-ray glows during winter thunderstorms in Japan, after which we performed a statistical analysis. Almost all the glows were detected in December, January, and February, when winter thunderstorms are frequent in the Hokuriku region, and 77% were detected at night. A typical T80 duration is minute-scale, 58.9 s on average. Half of the detected glows had a temporally symmetric (Gaussian-like) count-rate variation, which is suggestive of a stable electron accelerator passing above the detectors with a constant wind flow. One-quarter of the glows had a temporally asymmetric variation, implying multiple acceleration regions or one region with a complex shape. The remaining quarter terminated with lightning discharges. Energy spectra are well approximated by the power-law function with an exponential cutoff, whose average power-law index, cutoff energy, and energy flux are 0.50 MeV,

4.41 MeV, and  $8.4 \times 10^{-6}$  erg cm $^{-2}$  s $^{-1}$ , respectively. During glow detections, winds flow typically eastward, and the temperature is 4.6 °C on average. It will be worthwhile to investigate further the enriched data of the present catalog along with other observational, theoretical, and simulation works.

#### ACKNOWLEDGMENTS

Our deepest thanks go to the providers of the observation sites: K. Watarai and Kanazawa University High School; K. Yoneguchi and Kanazawa Izumigaoka High School; K. Kimura and Komatsu High School; K. Kitano and Science Hills Komatsu; K. Kono and Ishikawa Plating Industry Co., Ltd.; S. Kura and Kanazawa Nishi High School; and T. Matsui and Industrial Research Institute of Ishikawa. The BGO scintillation crystals are provided by Nuclear Experimental Group, Graduate School of Science, The University of Tokyo, thanks to H. Sakurai and M. Niikura. This project is supported by JSPS/MEXT KAKENHI Grants No. 15K05115, No. 16H06006, No. 18J13355, No. 18H01236, No. 19H00683, No. 20K22354, and No. 21H01116, the Hakubi project and SPIRITS 2017 of Kyoto University, the joint research program of the Institute for Cosmic Ray Research (ICRR), The University of Tokyo, RIKEN Special Postdoctoral Researchers program, and RIKEN Hakubi Research Fellowship program. The bootstrapping phase of this project was supported by a crowdfunding campaign named Thundercloud Project on the academic crowdfunding platform “academist.” The observation data and materials used to produce the figures in this paper are available on Mendeley Data [63]. The raw observation data will be provided upon request to the corresponding author. The background images in Fig. 1 are provided by the Geospatial Information Authority of Japan. The XRAIN data were provided by the Ministry of Land, Infrastructure, Transport and Tourism via the Data Integration and Analysis System (DIAS).

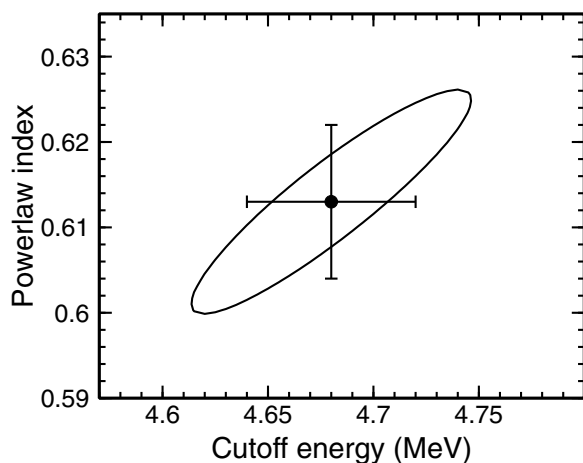


FIG. 16. A confidence region at one standard deviation of a fitting for the averaged spectrum, in the space of the power-law index and the cutoff energy. The cross marker also shows errors of one standard deviation of the two parameters but independently calculated.

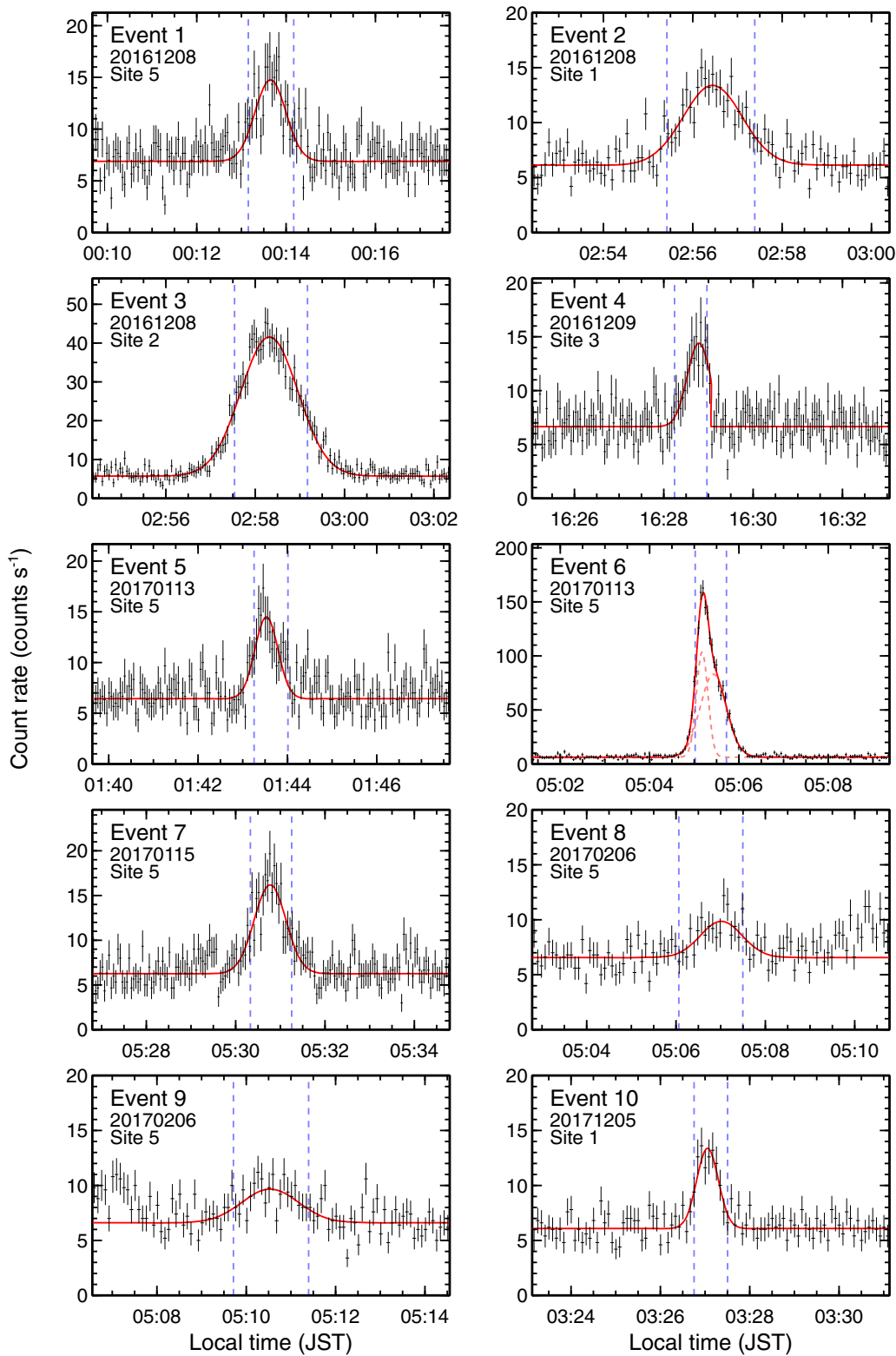


FIG. 17. Count-rate histories of Events 1–10 above 3 MeV. The local time (JST) is UTC+9 h. The blue dashed lines indicate the start and end of the T80 duration. The red solid lines show the fitting results with the Gaussian function. If the histories are fitted by multiple Gaussian functions, the components are overlaid by red dotted lines. The bin width is 3, 5, 3, 3, 3, 3, 3, 5, 5, and 5 s for Events 1–10, respectively.

**APPENDIX: COUNT-RATE HISTORIES AND INDIVIDUAL ENERGY SPECTRA**

As a gamma-ray glow catalog, count-rate histories of all the detected glows above 3 MeV are listed in Figs. 17–23.

In addition, the energy spectra of 28 bright glows are shown in Figs. 24–29, with response-folded and response-unfolded forms.

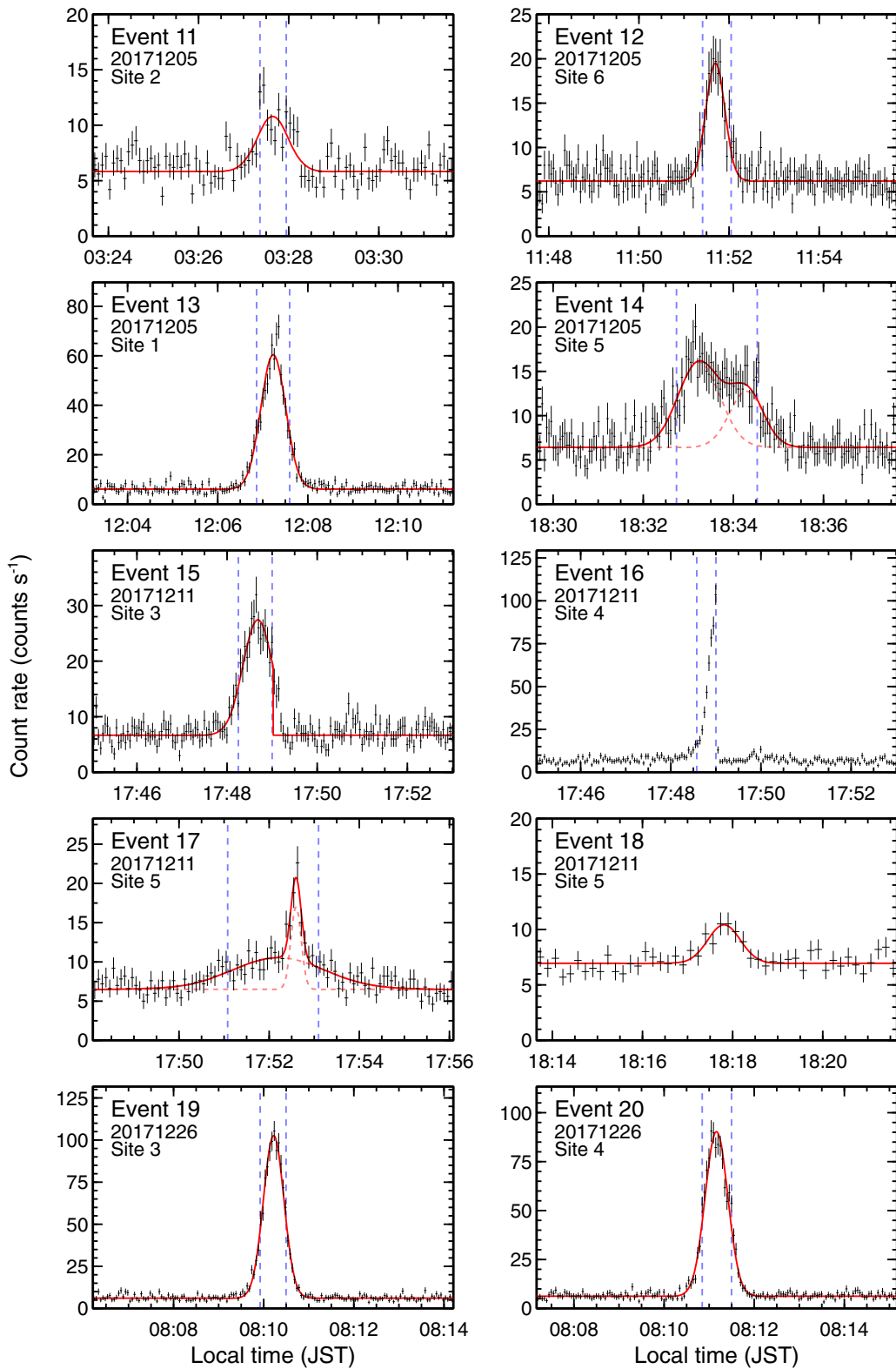


FIG. 18. Count-rate histories of Events 11–20 above 3 MeV in the same format as Fig. 17. The bin width is 5, 3, 3, 3, 3, 3, 5, 10, 3, and 3 s for Events 11–20, respectively.

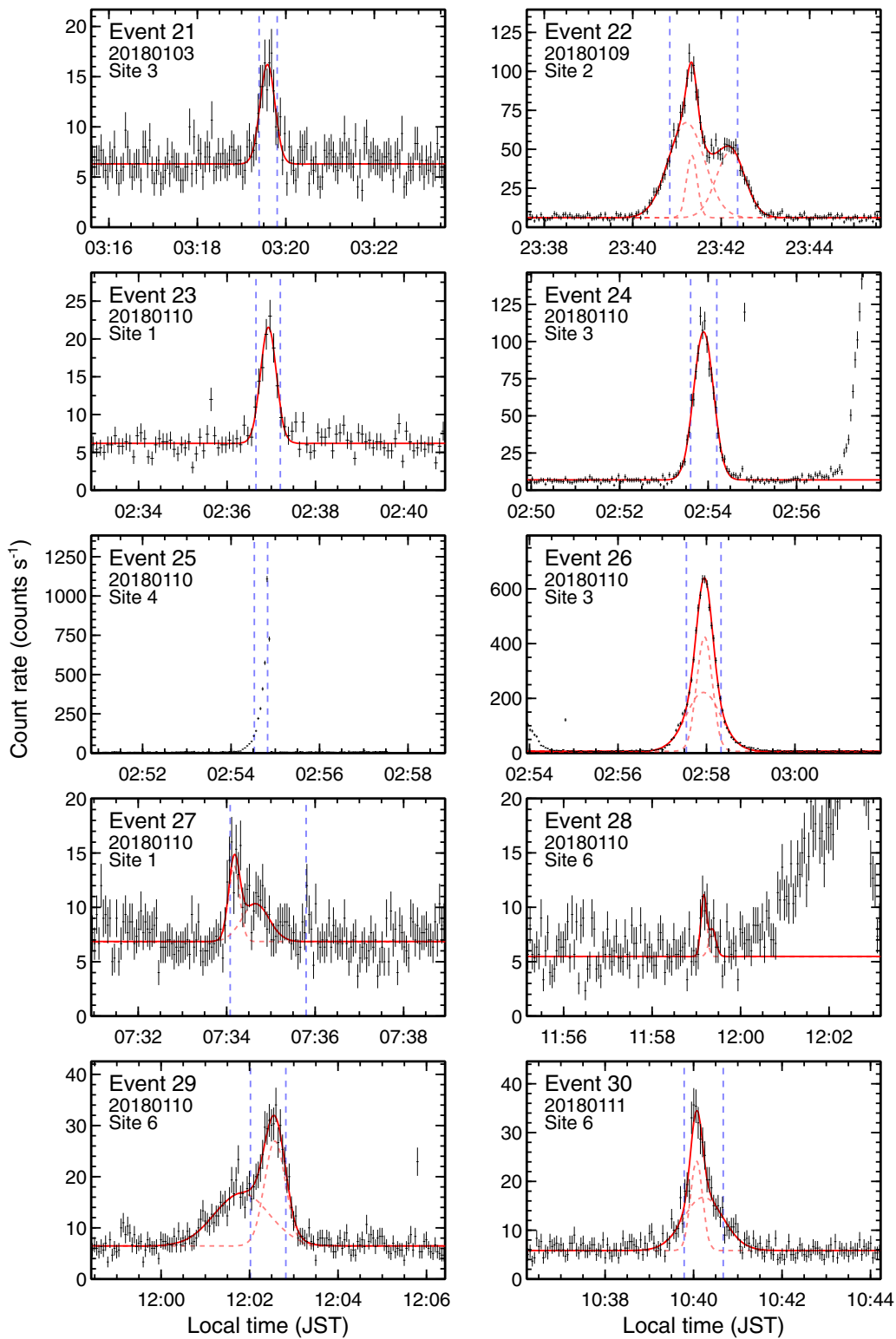


FIG. 19. Count-rate histories of Events 21–30 above 3 MeV in the same format as Fig. 17. The bin width is 3, 3, 5, 3, 3, 3, 3, 3, 3, and 3 s for Events 21–30, respectively.

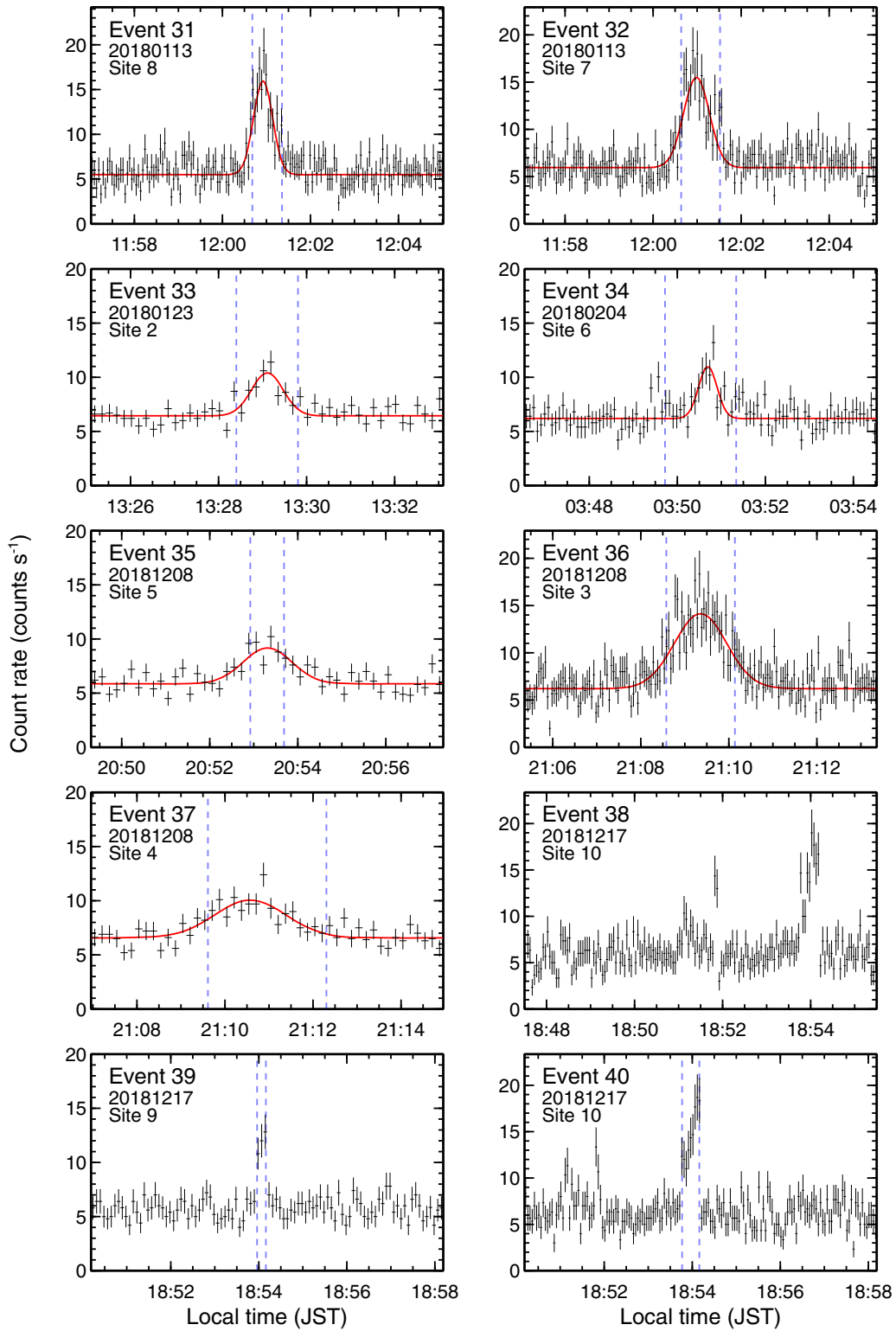


FIG. 20. Count-rate histories of Events 31–40 above 3 MeV in the same format as Fig. 17. The bin width is 3, 3, 10, 5, 10, 3, 10, 3, 5, and 3 s for Events 31–40, respectively.

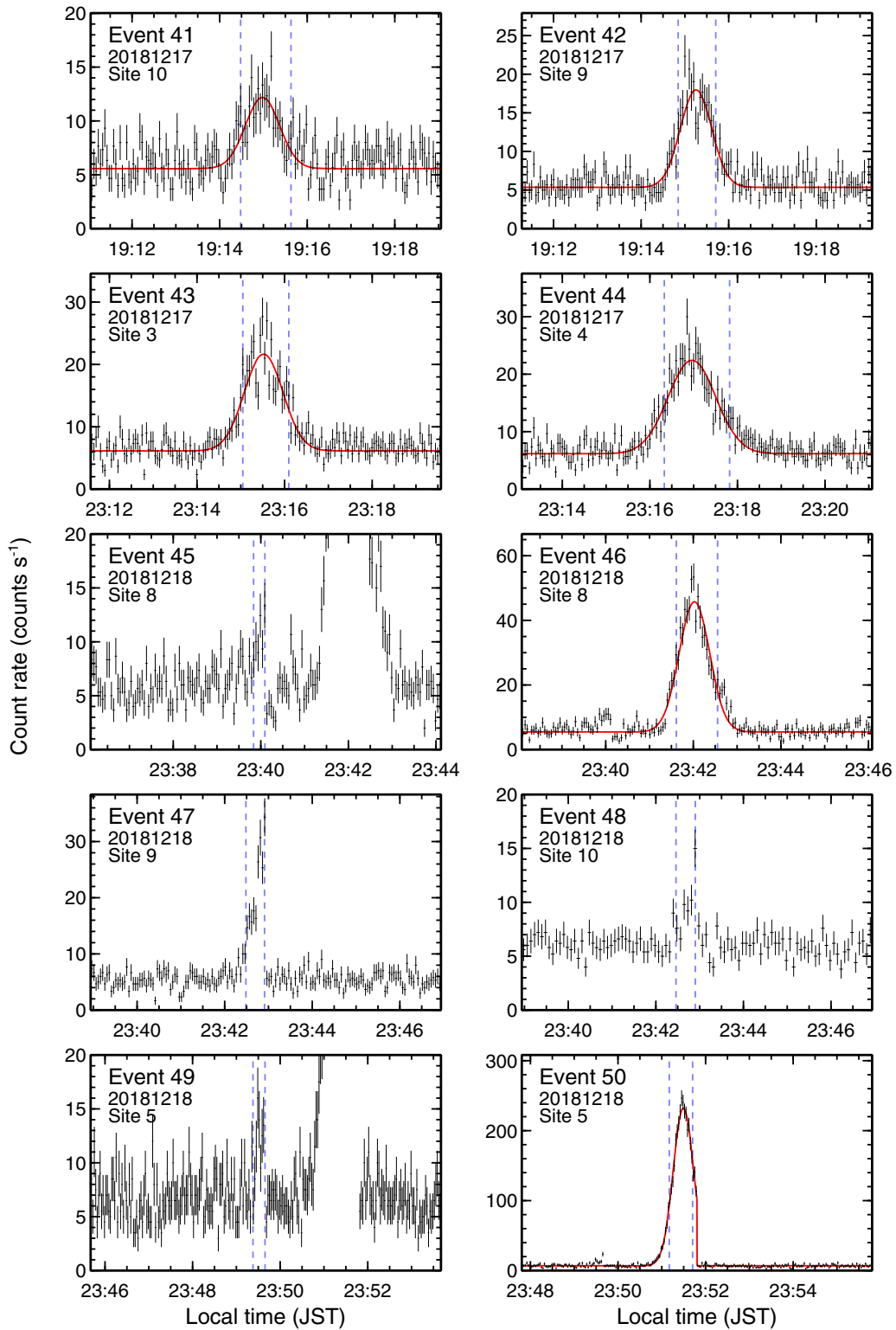


FIG. 21. Count-rate histories of Events 41–50 above 3 MeV in the same format as Fig. 17. The bin width is 3, 3, 3, 3, 3, 3, 3, 5, 2, and 2 s for Events 41–50, respectively.

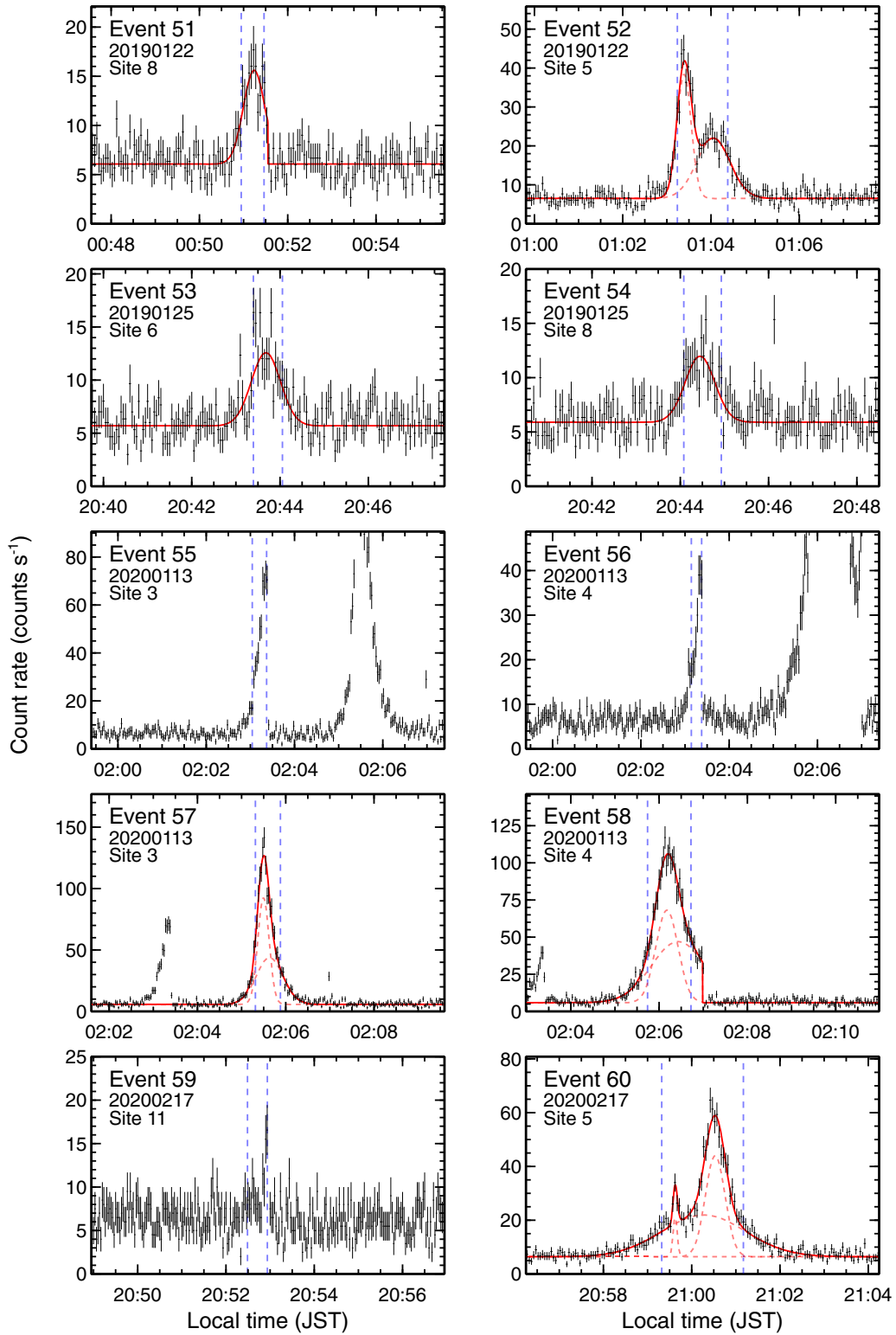


FIG. 22. Count-rate histories of Events 51–60 above 3 MeV in the same format as Fig. 17. The bin width is 3, 3, 3, 3, 2, 2, 2, 2, and 3 s for Events 51–60, respectively.

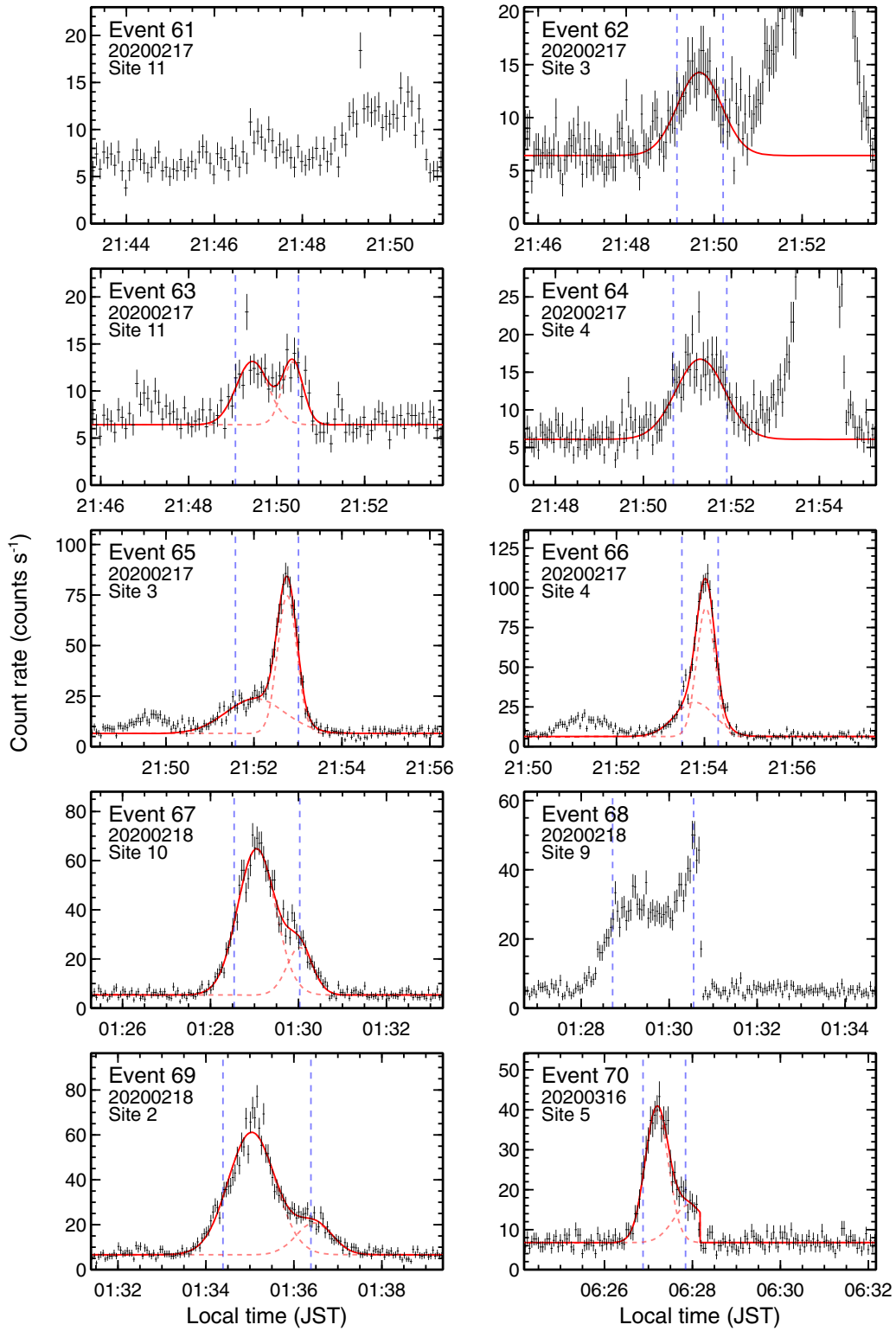


FIG. 23. Count-rate histories of Events 61–70 above 3 MeV in the same format as Fig. 17. The bin width is 5, 3, 5, 3, 3, 3, 3, 3, 3, and 3 s for Events 61–70, respectively.

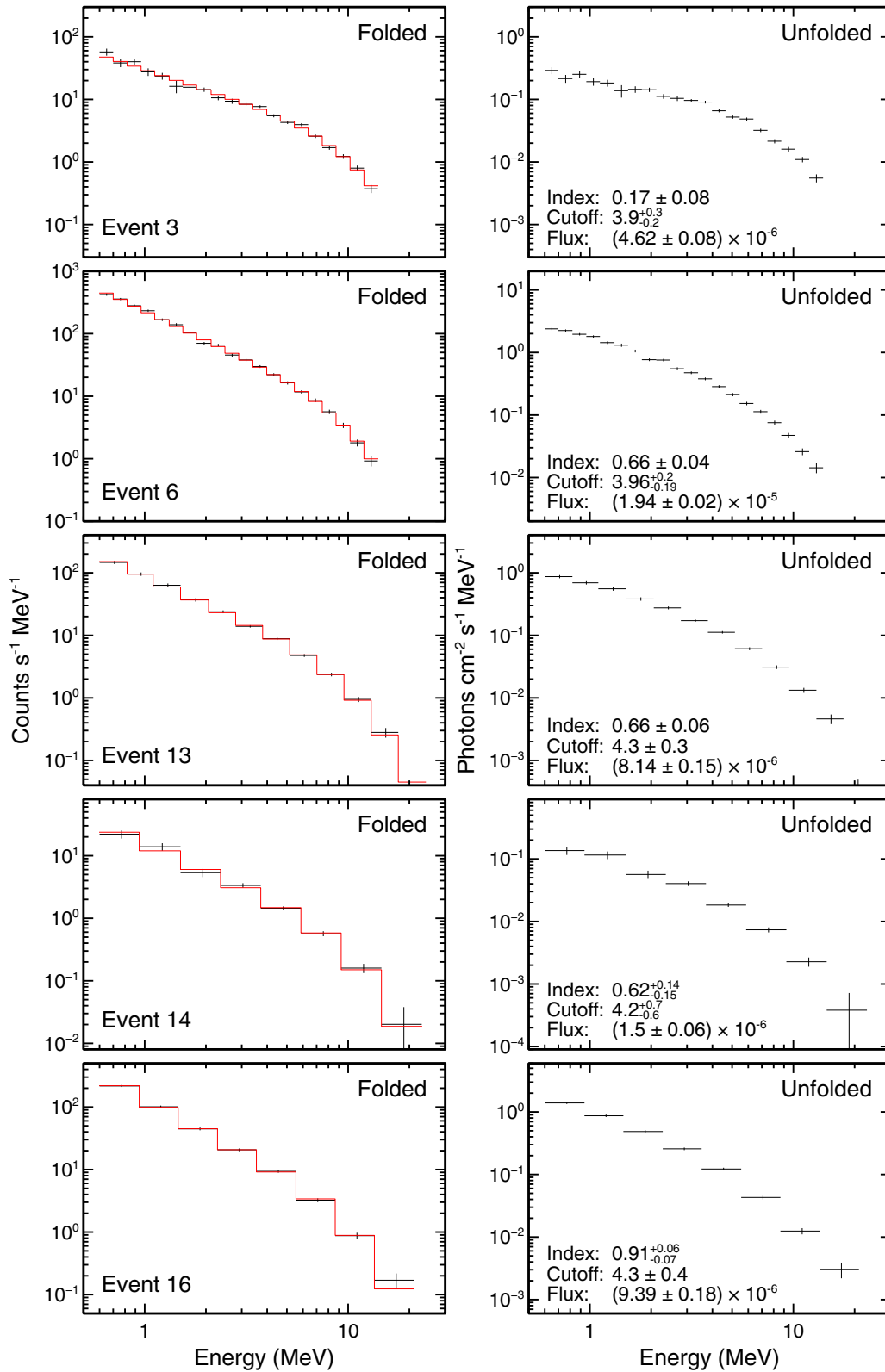


FIG. 24. Energy spectra of Events 3, 6, 13, 14, and 16. The left panels are in the count-rate space, and the right panels are in the photon-flux space produced by unfolding detector responses with XSPEC. The best-fit models are overlaid by the red-solid lines. The units of the cutoff energy and energy flux are MeV and  $\text{erg cm}^{-2} \text{s}^{-1}$ , respectively.

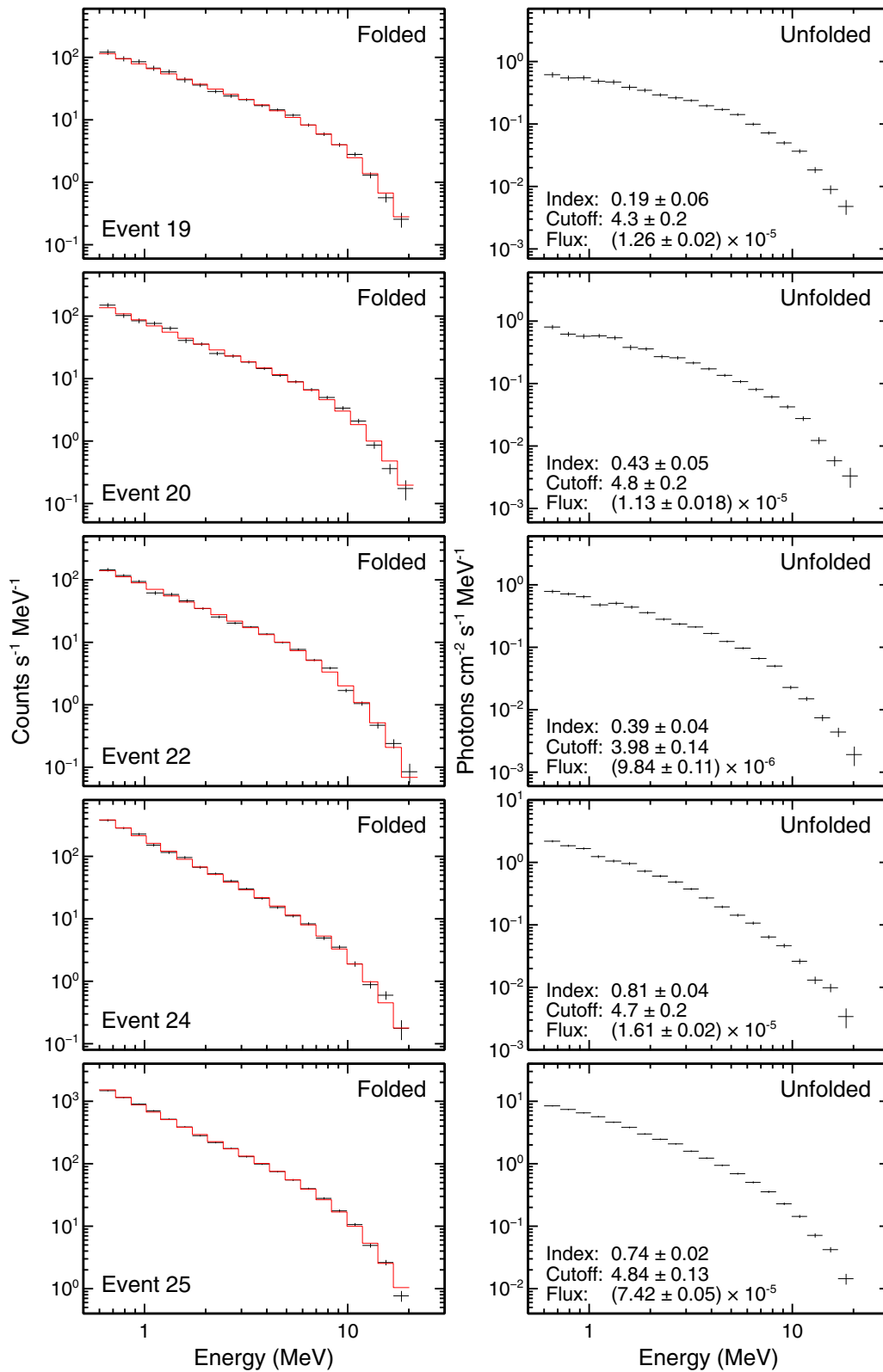


FIG. 25. Energy spectra of Events 19, 20, 22, 24, and 25 in the same format as Fig. 24.

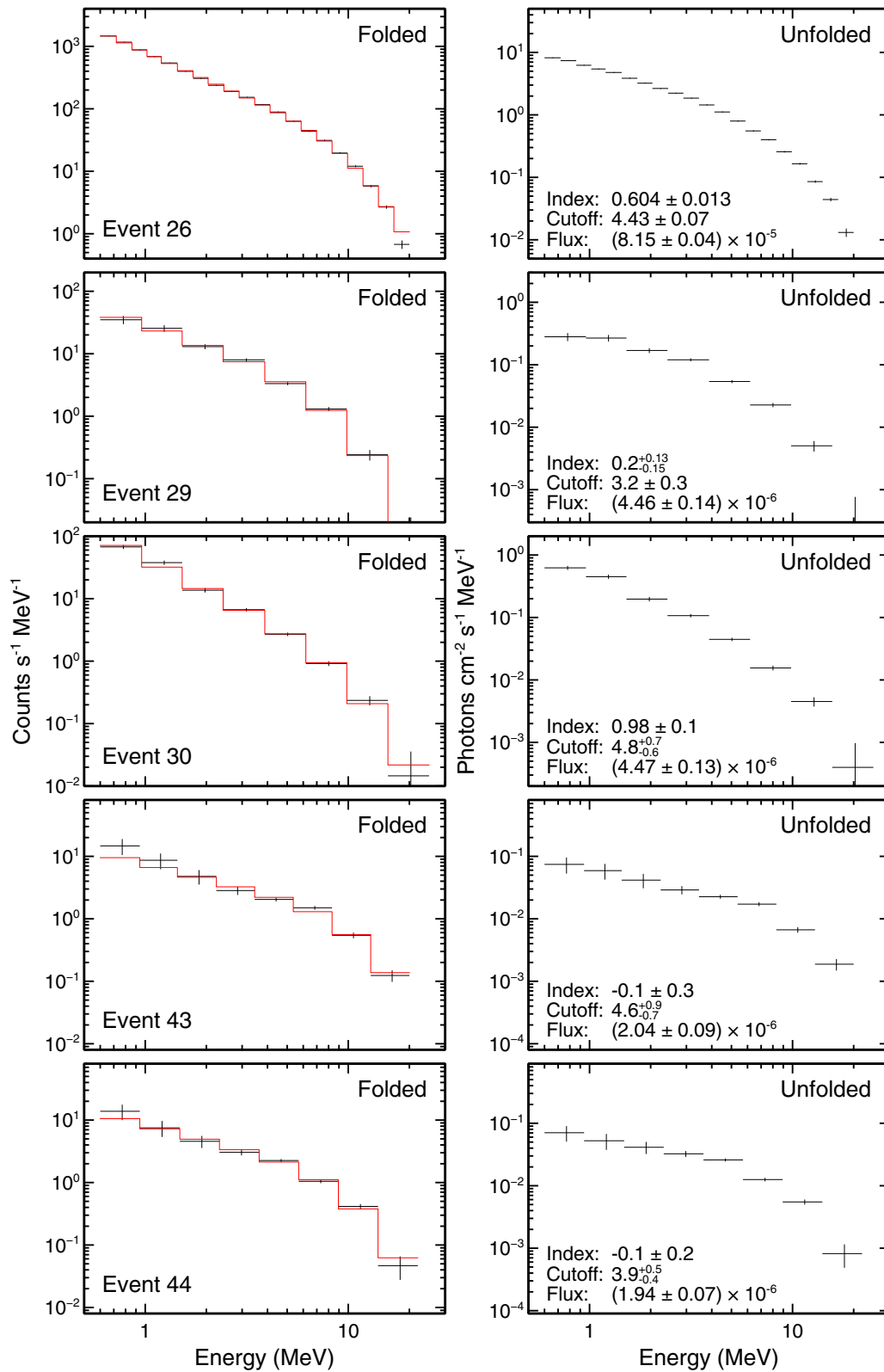


FIG. 26. Energy spectra of Events 26, 29, 30, 43, and 44 in the same format as Fig. 24.

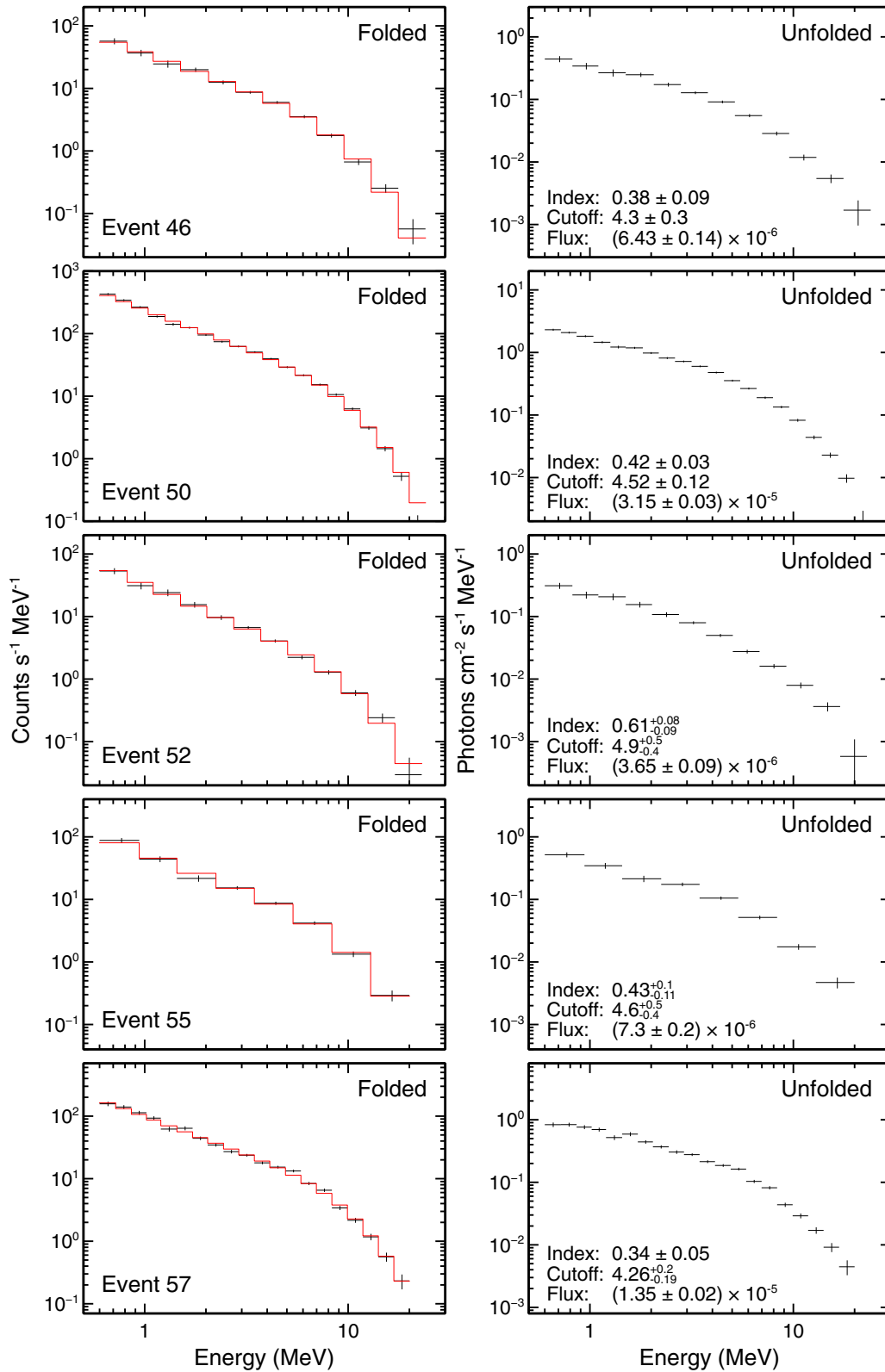


FIG. 27. Energy spectra of Events 46, 50, 52, 55, and 57 in the same format as Fig. 24.

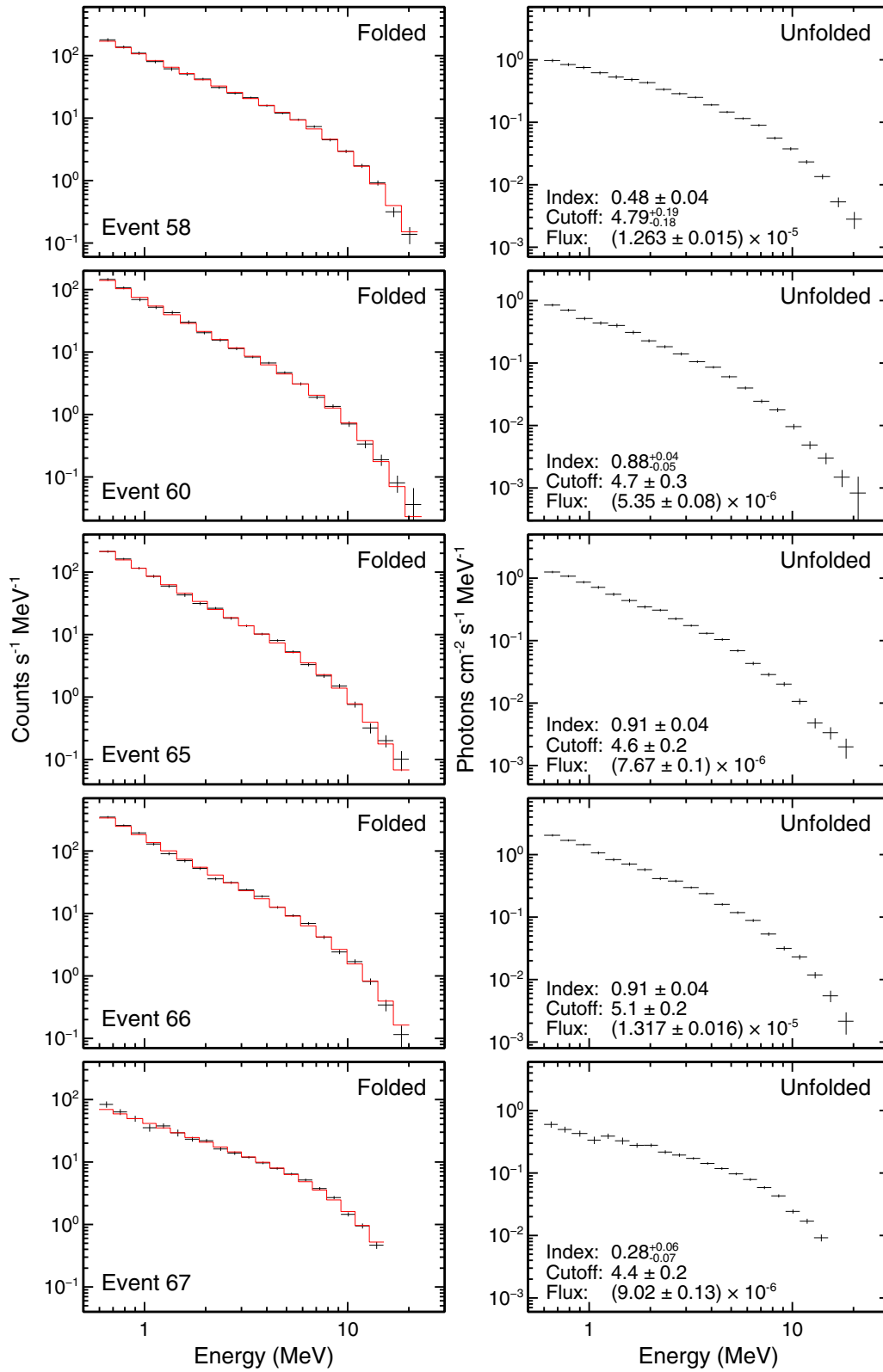


FIG. 28. Energy spectra of Events 58, 60, 65, 66, and 67 in the same format as Fig. 24.

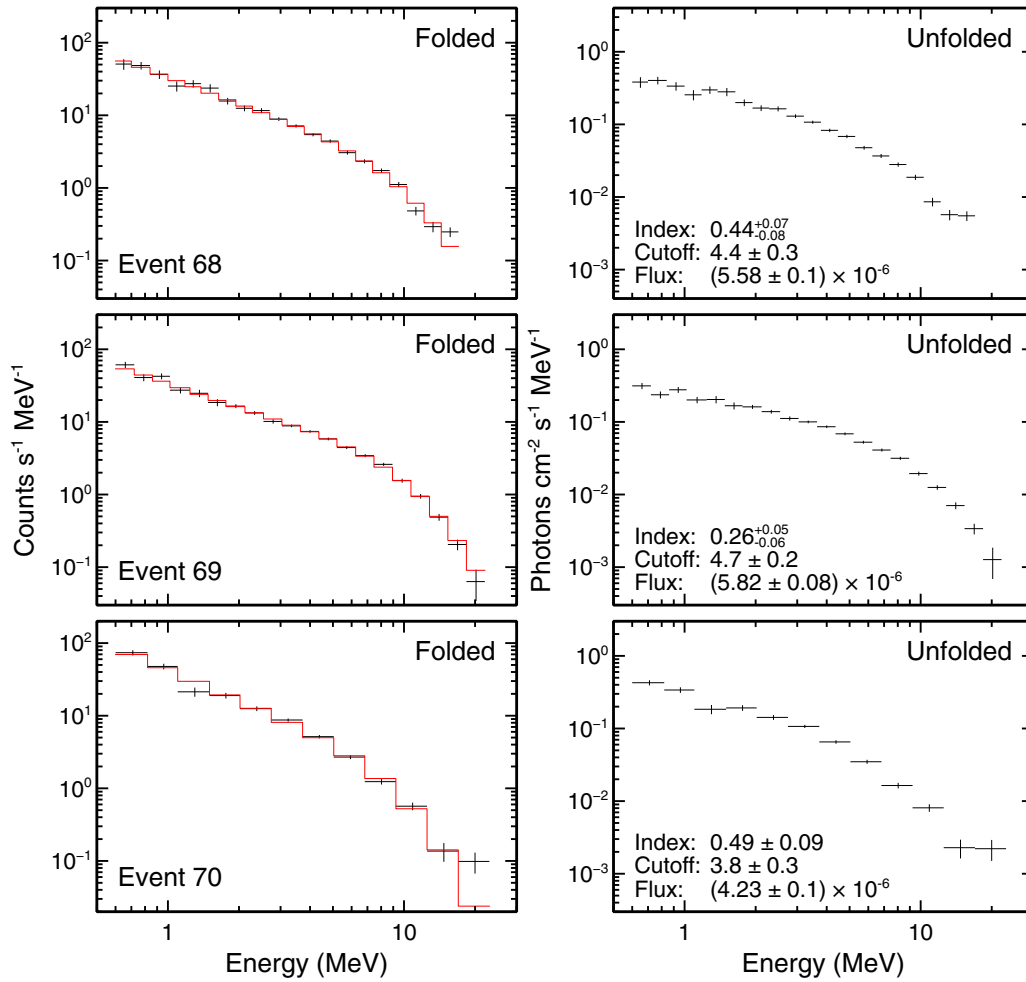


FIG. 29. Energy spectra of Events 68, 69, and 70 in the same format as Fig. 24.

[1] M. McCarthy and G. K. Parks, Further observations of x-rays inside thunderstorms, *Geophys. Res. Lett.* **12**, 393 (1985).

[2] T. Torii, M. Takeishi, and T. Hosono, Observation of gamma-ray dose increase associated with winter thunderstorm and lightning activity, *J. Geophys. Res.: Atmos.* **107**, ACL 2–1 (2002).

[3] H. Tsuchiya, T. Enoto, S. Yamada, T. Yuasa, M. Kawaharada, T. Kitaguchi, M. Kokubun, H. Kato, M. Okano, S. Nakamura, and K. Makishima, Detection of High-Energy Gamma Rays from Winter Thunderclouds, *Phys. Rev. Lett.* **99**, 165002 (2007).

[4] A. Chilingarian, A. Daryan, K. Arakelyan, A. Hovhannisyán, B. Mailyan, L. Melkumyan, G. Hovsepyan, S. Chilingaryan, A. Reymers, and L. Vanyan, Ground-based observations of thunderstorm-correlated fluxes of high-energy electrons, gamma rays, and neutrons, *Phys. Rev. D* **82**, 043009 (2010).

[5] H. Tsuchiya, T. Enoto, S. Yamada, T. Yuasa, K. Nakazawa, T. Kitaguchi, M. Kawaharada, M. Kokubun, H. Kato, M. Okano *et al.*, Long-duration  $\gamma$  ray emissions from 2007 and 2008 winter thunderstorms, *J. Geophys. Res.* **116**, D09113 (2011).

[6] Y. Wada, G. S. Bowers, T. Enoto, M. Kamogawa, Y. Nakamura, T. Morimoto, D. M. Smith, Y. Furuta, K. Nakazawa, T. Yuasa *et al.*, Termination of electron acceleration in thundercloud by intracloud/intercloud discharge, *Geophys. Res. Lett.* **45**, 5700 (2018).

[7] N. A. Kelley, D. M. Smith, J. R. Dwyer, M. Splitt, S. Lazarus, F. Martinez-McKinney, B. Hazelton, B. Grefenstette, A. Lowell, and H. K. Rassoul, Relativistic electron avalanches as a thunderstorm discharge competing with lightning, *Nat. Commun.* **6**, 7845 (2015).

[8] H. Tsuchiya, K. Hibino, K. Kawata, N. Hotta, N. Tateyama, M. Ohnishi, M. Takita, D. Chen, J. Huang, M. Miyasaka, I. Kondo, E. Takahashi, S. Shimoda, Y. Yamada, H. Lu, J. L. Zhang, X. X. Yu, Y. H. Tan, S. M. Nie, K. Munakata, T. Enoto, and K. Makishima, Observation of thundercloud-related gamma rays and neutrons in tibet, *Phys. Rev. D* **85**, 092006 (2012).

[9] A. Chilingarian, H. Mkrtchyan, G. Karapetyan, S. Chilingaryan, B. Sargsyan, and A. Arestakesyan, Catalog of 2017 thunderstorm ground enhancement (tge) events observed on aragats, *Sci. Rep.* **9**, 6253 (2019).

[10] G. K. Parks, B. H. Mauk, R. Spiger, and J. Chin, X-ray enhancements detected during thunderstorm and lightning activities, *Geophys. Res. Lett.* **8**, 1176 (1981).

[11] C. B. Moore, K. B. Eack, G. D. Aulich, and W. Rison, Energetic radiation associated with lightning stepped-leaders, *Geophys. Res. Lett.* **28**, 2141 (2001).

[12] N. Østgaard, H. J. Christian, J. E. Grove, D. Sarria, A. Mezentsev, P. Kochkin, N. Lehtinen, M. Quick, S. Al-Nussirat,

- E. Wulf *et al.*, Gamma-ray glow observations at 20 km altitude, *J. Geophys. Res.: Atmos.* **124**, 7236 (2019).
- [13] T. Torii, T. Sugita, S. Tanabe, Y. Kimura, M. Kamogawa, K. Yajima, and H. Yasuda, Gradual increase of energetic radiation associated with thunderstorm activity at the top of Mt. Fuji, *Geophys. Res. Lett.* **36**, L13804 (2009).
- [14] Y. Kuroda, S. Oguri, Y. Kato, R. Nakata, Y. Inoue, C. Ito, and M. Minowa, Observation of gamma ray bursts at ground level under the thunderclouds, *Phys. Lett. B* **758**, 286 (2016).
- [15] P. Kochkin, A. P. J. van Deursen, M. Marisaldi, A. Ursi, A. I. de Boer, M. Bardet, C. Allasia, J.-F. Boissin, F. Flourens, and N. Østgaard, In-flight observation of gamma ray glows by ILDAS, *J. Geophys. Res.: Atmos.* **122**, 12801 (2017).
- [16] P. Kochkin, D. Sarria, N. Lehtinen, A. Mezentsev, S. Yang, G. Genov, K. Ullaland, M. Marisaldi, N. Østgaard, H. J. Christian, J. E. Grove, M. Quick, S. Al-Nussirat, and E. Wulf, A rapid gamma-ray glow flux reduction observed from 20 km altitude, *J. Geophys. Res.: Atmos.* **126**, e2020JD033467 (2021).
- [17] A. Chilingarian and H. Mkrtchyan, Role of the lower positive charge region (lpcr) in initiation of the thunderstorm ground enhancements (tges), *Phys. Rev. D* **86**, 072003 (2012).
- [18] A. Chilingarian, Y. Khanikyants, E. Mareev, D. Pokhsaryan, V. A. Rakov, and S. Soghomonyan, Types of lightning discharges that abruptly terminate enhanced fluxes of energetic radiation and particles observed at ground level, *J. Geophys. Res.: Atmos.* **122**, 7582 (2017).
- [19] H. Tsuchiya, T. Enoto, T. Torii, K. Nakazawa, T. Yuasa, S. Torii, T. Fukuyama, T. Yamaguchi, H. Kato, M. Okano, M. Takita, and K. Makishima, Observation of an Energetic Radiation Burst From Mountain-Top Thunderclouds, *Phys. Rev. Lett.* **102**, 255003 (2009).
- [20] A. Shepetov, V. Antonova, O. Kalikulov, O. Kryakunova, A. Karashtin, V. Lutsenko, S. Mamina, K. Mukashev, V. Piscal, M. Ptitsyn, V. Ryabov, T. Sadykov, N. Saduev, N. Salikhov, Yu. Shlyugaev, L. Vildanova, V. Zhukov, and A. Gurevich, The prolonged gamma ray enhancement and the short radiation burst events observed in thunderstorms at tien shan, *Atmos. Res.* **248**, 105266 (2021).
- [21] Y. Wada, T. Enoto, M. Kubo, K. Nakazawa, T. Shinoda, D. Yonetoku, T. Sawano, T. Yuasa, T. Ushio, Y. Sato, G. S. Diniz, and H. Tsuchiya, Meteorological aspects of gamma-ray glows in winter thunderstorms, *Geophys. Res. Lett.* **48**, e2020GL091910 (2021).
- [22] T. Yuasa, Y. Wada, T. Enoto, Y. Furuta, H. Tsuchiya, S. Hisadomi, Y. Tsuji, K. Okuda, T. Matsumoto, K. Nakazawa, K. Makishima, S. Miyake, and Y. Ikkatai, Thundercloud project: Exploring high-energy phenomena in thundercloud and lightning, *Prog. Theor. Exp. Phys.* **2020**, 103H01 (2020).
- [23] Y. Wada, T. Enoto, Y. Nakamura, T. Morimoto, M. Sato, T. Ushio, K. Nakazawa, T. Yuasa, D. Yonetoku, T. Sawano *et al.*, High peak-current lightning discharges associated with downward terrestrial gamma-ray flashes, *J. Geophys. Res.: Atmos.* **125**, e2019JD031730 (2020).
- [24] Y. Wada, T. Enoto, Y. Nakamura, Y. Furuta, T. Yuasa, K. Nakazawa, T. Morimoto, M. Sato, T. Matsumoto, D. Yonetoku, T. Sawano, H. Sakai, M. Kamogawa, T. Ushio, K. Makishima, and H. Tsuchiya, Gamma-ray glow preceding downward terrestrial gamma-ray flash, *Commun. Phys.* **2**, 67 (2019).
- [25] S. Hisadomi, K. Nakazawa, Y. Wada, Y. Tsuji, T. Enoto, T. Shinoda, T. Morimoto, Y. Nakamura, T. Yuasa, and H. Tsuchiya, Multiple gamma-ray glows and a downward TGF observed from nearby thunderclouds, *J. Geophys. Res.: Atmos.* **126**, e2021JD034543 (2021).
- [26] N. Kitagawa and K. Michimoto, Meteorological and electrical aspects of winter thunderclouds, *J. Geophys. Res.* **99**, 10713 (1994).
- [27] V. A. Rakov and M. A. Uman, *Lightning: Physics and Effects* (Cambridge University Press, Cambridge, 2003).
- [28] T. Takahashi, Riming electrification as a charge generation mechanism in thunderstorms, *J. Atmos. Sci.* **35**, 1536 (1978).
- [29] E. R. Williams, The tripole structure of thunderstorms, *J. Geophys. Res.* **94**, 13151 (1989).
- [30] Y. Goto and K. Narita, Observations of winter lightning to an isolate tower, *Res. Lett. Atmos. Electr.* **12**, 57 (1992).
- [31] T. Torii, T. Sugita, M. Kamogawa, Y. Watanabe, and K. Kusunoki, Migrating source of energetic radiation generated by thunderstorm activity, *Geophys. Res. Lett.* **38**, L24801 (2011).
- [32] H. Tsuchiya, T. Enoto, K. Iwata, S. Yamada, T. Yuasa, T. Kitaguchi, M. Kawaharada, K. Nakazawa, M. Kokubun, H. Kato, M. Okano, T. Tamagawa, and K. Makishima, Hardening and Termination of Long-Duration  $\gamma$  Rays Detected Prior to Lightning, *Phys. Rev. Lett.* **111**, 015001 (2013).
- [33] D. Umemoto, H. Tsuchiya, T. Enoto, S. Yamada, T. Yuasa, M. Kawaharada, T. Kitaguchi, K. Nakazawa, M. Kokubun, H. Kato, M. Okano, T. Tamagawa, and K. Makishima, On-ground detection of an electron-positron annihilation line from thunderclouds, *Phys. Rev. E* **93**, 021201(R) (2016).
- [34] T. Enoto, Y. Wada, Y. Furuta, K. Nakazawa, T. Yuasa, K. Okuda, K. Makishima, M. Sato, Y. Sato, T. Nakano *et al.*, Photonuclear reactions triggered by lightning discharge, *Nature (London)* **551**, 481 (2017).
- [35] G. J. Fishman, P. N. Bhat, R. Mallozzi, J. M. Horack, T. Koshut, C. Kouveliotou, G. N. Pendleton, C. A. Meegan, R. B. Wilson, W. S. Paciesas *et al.*, Discovery of intense gamma-ray flashes of atmospheric origin, *Science* **264**, 1313 (1994).
- [36] D. M. Smith, L. I. Lopez, R. P. Lin, and C. P. Barrington-Leigh, Terrestrial gamma-ray flashes observed up to 20 mev, *Science* **307**, 1085 (2005).
- [37] M. Tavani, M. Marisaldi, C. Labanti, F. Fuschino, A. Argan, A. Trois, P. Giommi, S. Colafrancesco, C. Pittori, F. Palma *et al.*, Terrestrial Gamma-Ray Flashes as Powerful Particle Accelerators, *Phys. Rev. Lett.* **106**, 018501 (2011).
- [38] N. Østgaard, T. Neubert, V. Reglero, K. Ullaland, S. Yang, G. Genov, M. Marisaldi, A. Mezentsev, P. Kochkin, N. Lehtinen *et al.*, First 10 months of tgf observations by asim, *J. Geophys. Res.: Atmos.* **124**, 14024 (2019).
- [39] S. Foley, G. Fitzpatrick, M. S. Briggs, V. Connaughton, D. Tierney, S. McBreen, J. R. Dwyer, V. L. Chaplin, P. N. Bhat, D. Byrne *et al.*, Pulse properties of terrestrial gamma-ray flashes detected by the fermi gamma-ray burst monitor, *J. Geophys. Res.: Space Phys.* **119**, 5931 (2014).
- [40] M. Marisaldi, F. Fuschino, C. Labanti, M. Galli, F. Longo, E. Del Monte, G. Barbiellini, M. Tavani, A. Giuliani, E. Moretti *et al.*, Detection of terrestrial gamma ray flashes up to 40 MeV by the AGILE satellite, *J. Geophys. Res.* **115**, A00E13 (2010).
- [41] B. G. Mailyan, M. S. Briggs, E. S. Cramer, G. Fitzpatrick, O. J. Roberts, M. Stanbro, V. Connaughton, S. McBreen, P. N. Bhat, and J. R. Dwyer, The spectroscopy of individual terrestrial gamma-ray flashes: Constraining the source properties, *J. Geophys. Res.: Space Phys.* **121**, 11346 (2016).

- [42] M. S. Briggs, G. J. Fishman, V. Connaughton, P. N. Bhat, W. S. Paciesas, R. D. Preece, C. Wilson-Hodge, V. L. Chaplin, R. M. Kippen, A. von Kienlin *et al.*, First results on terrestrial gamma ray flashes from the fermi gamma-ray burst monitor, *J. Geophys. Res.* **115**, A07323 (2010).
- [43] T. Neubert, N. Østgaard, V. Reglero, O. Chanrion, M. Heumesser, K. Dimitriadou, F. Christiansen, C. Budtz-Jørgensen, I. Kuvvetli, I. L. Rasmussen *et al.*, A terrestrial gamma-ray flash and ionospheric ultraviolet emissions powered by lightning, *Science* **367**, 183 (2020).
- [44] J. R. Dwyer, M. M. Schaal, E. Cramer, S. Arabshahi, N. Liu, H. K. Rassoul, J. D. Hill, D. M. Jordan, and M. A. Uman, Observation of a gamma-ray flash at ground level in association with a cloud-to-ground lightning return stroke, *J. Geophys. Res.* **117**, A10303 (2012).
- [45] B. M. Hare, M. A. Uman, J. R. Dwyer, D. M. Jordan, M. I. Biggerstaff, J. A. Caicedo, F. L. Carvalho, R. A. Wilkes, D. A. Kotovsky, W. R. Gameraota *et al.*, Ground-level observation of a terrestrial gamma ray flash initiated by a triggered lightning, *J. Geophys. Res.: Atmos.* **121**, 6511 (2016).
- [46] M. D. Tran, V. A. Rakov, S. Mallick, J. R. Dwyer, A. Nag, and S. Heckman, A terrestrial gamma-ray flash recorded at the lightning observatory in gainesville, florida, *J. Atmos. Sol. Terr. Phys.* **136**, 86 (2015).
- [47] Y. Wada, T. Enoto, K. Nakazawa, Y. Furuta, T. Yuasa, Y. Nakamura, T. Morimoto, T. Matsumoto, K. Makishima, and H. Tsuchiya, Downward Terrestrial Gamma-Ray Flash Observed in a Winter Thunderstorm, *Phys. Rev. Lett.* **123**, 061103 (2019).
- [48] D. M. Smith, G. S. Bowers, M. Kamogawa, D. Wang, T. Ushio, J. Ortberg, J. R. Dwyer, and M. Stock, Characterizing upward lightning with and without a terrestrial gamma-ray flash, *J. Geophys. Res.: Atmos.* **123**, 11321 (2018).
- [49] A. V. Gurevich, G. M. Milikh, and R. Roussel-Dupre, Runaway electron mechanism of air breakdown and preconditioning during a thunderstorm, *Phys. Lett. A* **165**, 463 (1992).
- [50] L. P. Babich, E. N. Donskoy, R. I. Il'kaev, I. M. Kutsyk, and R. A. Roussel-Dupre, Fundamental parameters of a relativistic runaway electron avalanche in air, *Plasma Phys. Rep.* **30**, 616 (2004).
- [51] J. R. Dwyer, A fundamental limit on electric fields in air, *Geophys. Res. Lett.* **30**, 2055 (2003).
- [52] J. R. Dwyer, Relativistic breakdown in planetary atmospheres, *Phys. Plasmas* **14**, 042901 (2007).
- [53] A. Chilingarian, G. Hovsepyan, and L. Vanyan, On the origin of the particle fluxes from the thunderclouds: Energy spectra analysis, *Europhys. Lett.* **106**, 59001 (2014).
- [54] E. S. Cramer, B. G. Mailyan, S. Celestin, and J. R. Dwyer, A simulation study on the electric field spectral dependence of thunderstorm ground enhancements and gamma ray glows, *J. Geophys. Res.: Atmos.* **122**, 4763 (2017).
- [55] G. S. Bowers, W. Blaine, X.-M. Shao, B. Dings, D. M. Smith, M. Schneider, F. Martinez-McKinney, M. P. McCarthy, S. BenZvi, L. Nellen, and N. Fraija, Combining Cherenkov and scintillation detector observations with simulations to deduce the nature of high-energy radiation excesses during thunderstorms, *Phys. Rev. D* **100**, 043021 (2019).
- [56] Z.-B. Zhang and C.-S. Choi, An analysis of the durations of swift gamma-ray bursts, *Astron. Astrophys.* **484**, 293 (2008).
- [57] K. A. Arnaud, XSPEC: The First Ten Years, in *Astronomical Data Analysis Software and Systems V*, Astronomical Society of the Pacific Conference Series Vol. 101, edited by G. H. Jacoby and J. Barnes (Astronomical Society of the Pacific, San Francisco, CA, 1996), p. 17.
- [58] S. Agostinelli, J. Allison, K. Amako, J. Apostolakis, H. Araujo, P. Arce, M. Asai, D. Axen, S. Banerjee, G. Barrant *et al.*, Geant4—a simulation toolkit, *Nucl. Instrum. Methods Phys. Res., Sec. A* **506**, 250 (2003).
- [59] J. Allison, K. Amako, J. Apostolakis, H. Araujo, P. Arce Dubois, M. Asai, G. Barrant, R. Capra, S. Chauvie, R. Chytracsek *et al.*, Geant4 developments and applications, *IEEE Trans. Nucl. Sci.* **53**, 270 (2006).
- [60] J. Allison, K. Amako, J. Apostolakis, P. Arce, M. Asai, T. Aso, E. Bagli, A. Bagulya, S. Banerjee, G. Barrant *et al.*, Recent developments in geant4, *Nucl. Instrum. Methods Phys. Res., Sec. A* **835**, 186 (2016).
- [61] J. R. Dwyer, D. M. Smith, and S. A. Cummer, High-energy atmospheric physics: Terrestrial gamma-ray flashes and related phenomena, *Space Sci. Rev.* **173**, 133 (2012).
- [62] A. Chilingarian, G. Hovsepyan, T. Karapetyan, G. Karapetyan, L. Kozliner, H. Mkrtchyan, D. Aslanyan, and B. Sargsyan, Structure of thunderstorm ground enhancements, *Phys. Rev. D* **101**, 122004 (2020).
- [63] <https://doi.org/10.17632/nrtmmbx3jg.1>.